EFFECT OF CHROMIUM SUBSTITUTION ON THE STRUCTURAL, ELECTRICAL, AND MAGNETIC PROPERTIES OF Ni-Mn-Zn FERRITES

By

Siyara Bibi

M.Phil in Physics

Student ID: 15MPHY005P

A thesis submitted in partial fulfillment of the requirements for the degree of

MASTER of PHILOSOPHY in Physics

Department of Physics

CHITTAGONG UNIVERSITY OF ENGINEERING AND TECHNOLOGY

June 2025

Declaration

I hereby declare that the work contained in this Thesis has not been previously submitted to meet requirements for an award at this or any other higher education institution. To the best of my knowledge and belief, the Thesis contains no material previously published or written by another person except where due reference is cited. Furthermore, the Thesis complies with PLAGIARISM and ACADEMIC INTEGRITY regulation of CUET.

Siyara Bibi

15MPHY005P

Department of Physics

Chittagong University of Engineering & Technology (CUET)

Dedication

Dedicated

To

My Parents

List of Publications

List of Conferences Attended

1. **Effect of Chromium Substitutions on the Structural, DC Resistivity and Dielectric properties of $Ni_{0.6}Mn_{0.2}Zn_{0.2}Fe_{2-x}Cr_xO_4$ ferrites, S. Bibi, M.N.I. Khan, S.M. Hoque, and M.M. Uddin, and F.U.Z Chowdhury; "Conference on Weather Forecasting & Advances in Physics", 11-12 May 2018, organized by Dept. of Physics, Khulna University of Engineering & Technology (KUET).**
2. **Effect of Chromium substitutions on the structural, DC resistivity, and dielectric properties of $Ni_{0.6}Mn_{0.2}Zn_{0.2}Fe_{2-x}Cr_xO_4$ ferrites, S. Bibi, M.N.I. Khan, S.M. Hoque, F.U.Z. Chowdhury, M.A. Ali. "5th International conference on Physics for Sustainable Development & Technology (ICPSDT-2023)" 7-8 September, 2023; organized by Department of Physics, CUET.**

Approval/ Declaration by the Supervisor(s)

This is to certify that Siyara BiBi bearing roll number 15MPHY005P has carried out this research work under my/our supervision, and that she has fulfilled the relevant Academic Ordinance of the Chittagong University of Engineering and Technology, so that she is qualified to submit the following Thesis in the application for the degree of MASTER of PHILOSOPHY in PHYSICS. Furthermore, the Thesis complies with the PLAGIARISM and ACADEMIC INTEGRITY regulation of CUET.

Dr. Md. Ashraf Ali

Professor

Department of Physics

Chittagong University of Engineering & Technology

Acknowledgement

At first, I would like to thank the Almighty Allah for granting me the courage, wisdom, and the chance to do this research project and successfully finish it.

Many people's efforts and support have gone into my thesis, and words cannot adequately convey how grateful I am on the inside. In addition to the educational experience I had, these kinds of people's company have greatly enhanced and impacted my life.

I am deeply grateful to my supervisor Dr. Md. Ashraf Ali, Professor, Department of Physics, Chittagong University of Engineering and Technology (CUET). He guided me with his characteristic wisdom and patience and bore all my limitations with the utmost affection. Without his tremendous guidance, this task would not have been feasible.

I am deeply indebted to Dr. Faruque Uz-Zaman Chowdhury, Professor, Department of Physics, Chittagong University of Engineering and Technology (CUET). Initially he acts as supervisor and there after he acts as co-supervisor of my research work.

I am deeply grateful to my co-supervisor, Dr. Mohammed Nazrul Islam Khan, Principal Scientific Officer, Materials Science Division, Atomic Energy Centre, Dhaka (AECD), for his continuous support and valuable guidance.

It is a great pleasure of mine to express my heart felt thanks to Professor Dr. H.M.A.R. Maruf, Head, Department of Physics, CUET for his cordial inspiration during the progress at each step of this work.

I want to express my sincere gratitude to Dr. Md. Mohi Uddin, Professor, Department of Physics, Chittagong University of Engineering and Technology (CUET) for his kind encouragement and recommendations at every stage of this project's progress.

I am also grateful to my respectable teachers Prof. Dr. Mohammad Belal Hossen, Prof. Dr. Swapan Kumar Roy, Prof. Dr. Nusrat Jahan, Prof. Dr. Animesh Kumar Chakraborty, Associate Prof. Dr. Md. Mukter Hossain Department of Physics, CUET who suggested valuable guidance during the whole process.

I am extremely grateful to all the people at the Materials Science Division of AEC, Dhaka for their lab facilities, Specially Dr. Sheikh Manjura Hoque (CSO and Head, Materials Science Division of AECD). This study was made possible by the kind and generous assistance of Md. Kamrul Hasan, Zarna Begum, Alhamra Parveen, Halima Sadia, Nazmun nahar Begum, and Md. Sohel.

I would especially want to thank my sister like friend Mithila Das for her assistance with this research and also thank Md. Sohel, Trayee Barua, Farhana Sultana, Anny Chowdhury, Prianka Borua due to their friendly cooperation.

I would like to thank the CUET Department of Physics for providing the required authorization and technical assistance for this effort.

Finally, I am immensely grateful to my elder brother Md. Abdul Zabber, and elder sister Amana Akter for their encouragement and support. I am also thankful to my family and well-wishers for their support.

Abstract

Cr^{3+} substituted Ni-Mn-Zn, a chemical composition of ferrites that includes $Ni_{0.6}Mn_{0.2}Zn_{0.2}Cr_xFe_{2-x}O_4$ ferrites (where x = 0.00, 0.05, 0.10, 0.15, 0.20), were synthesized via the solid-state reaction method. Inside a muffle furnace, these samples are heated to 1100°C for four hours and then left to cool down naturally. The ferrites were then further studied using X-ray diffraction (XRD), Scanning Electron Microscope (SEM), Impedance analyzer, and Vibrating Sample Magnetometer (VSM). The XRD data confirmed the formation of a cubic spinel structure without secondary phases. A reduction of the lattice constant due to Cr^{3+} presence is observed because of having smaller Cr ions (0.62Å) than Fe ions (0.645Å). The SEM images confirmed the homogenous distribution of grains, where the grain sizes of the Cr^{3+}-substituted composition are found to be less than that of the Ni-Mn-Zn basic composition, except for x=0.10. The Cr^{3+}-substituted compositions exhibit a larger dielectric constant than the x=0.0 composition. The AC resistivity value is also less for the Cr^{3+}-substituted compositions. The VSM was utilized to investigate the magnetic properties. The saturation magnetization, remanent magnetization, and coercive field were significantly influenced by the Cr^{3+} substitution because Cr^{3+} has a lower magnetic moment than Fe^{3+}. A decrease in magnetic permeability has also been observed owing to the Cr^{3+} substitution.

বিমূর্ত

আমরা Ni-Mn-Zn ferrites এর Fe^{3+} কে Cr^{3+} দ্বারা প্রতিস্থাপিত করে $Ni_{0.6}Mn_{0.2}Zn_{0.2}Cr_xFe_{2-x}O_4$ (যেখানে x = 0.00, 0.05, 0.10, 0.15, 0.20) ferrites গুলো double sintering প্রকিয়ায় প্রস্তুত করা হয়েছে। এই নমুনাগুলি 1100 ডিগ্রি সেলসিয়াসে 4 ঘন্টার জন্য একটি মাফল ফার্নেসে sintering করা হয় এবং স্বাভাবিক তাপমাত্রায় ঠান্ডা করা হয়। এক্স-রে ডিফ্রেকশন (XRD), স্ক্যানিং ইলেক্ট্রন মাইক্রোস্কোপ (SEM), ইম্পিডেন্স অ্যানালাইজার এবং ভাইব্রেটিং স্যাম্পল ম্যাগনেটোমিটার (VSM) ব্যবহার করে ফেরাইটের কাঠামো গত, বৈদ্যুতিক এবং চৌম্বকীয় বৈশিষ্ট্য গুলি পর্যবেক্ষণ করা হয়েছে। এক্স আর ডি (XRD) তথ্য single-phase cubic spinel structure নিশ্চিত করেছে। Fe (0.645 Å) আয়নগুলির তুলনায় Cr (0.62 Å) এর আয়নিক ব্যাসার্ধ ছোট হওয়ার কারনে Cr উপাদানের সাথে সাথে ল্যাটিস ধ্রুবক হ্রাস পেয়েছে। SEM চিত্র গুলি grains সুষম বণ্টনের বিষয়টি নিশ্চিত করেছে, যেখানে Cr^{3+} প্রতিস্থাপনের ফলে grains এর আকার x=0.10 ব্যতীত Ni-Mn-Zn মৌলিক গঠনের তুলনায় কম পাওয়া গেছে। Cr^{3+} প্রতিস্থাপিত কম্পোজিশন গুলির ডাই ইলেক্ট্রিক ধ্রুবক x = 0.0 কম্পোজিশনের চেয়ে বেশি। Cr^{3+} প্রতিস্থাপিত কম্পোজিশন গুলির জন্যও এসি প্রতিরোধকের মান কম পাওয়া গেছে। চৌম্বকীয় বৈশিষ্ট্যগুলি VSM দ্বারা পর্যবেক্ষণ করা হয়েছে। Fe^{3+} এর তুলনায় Cr^{3+} এর magnetic moment কম হওয়ার কারণে saturation magnetization, remanent magnetization, and coercive field এর উপর Cr^{3+} প্রতিস্থাপনের একটি উল্লেখযোগ্য প্রভাব লক্ষ্য করা গেছে। Cr^{3+} প্রতিস্থাপনের কারণে magnetic permeability ও হ্রাস পেয়েছে।

Table of Contents

List of Figures

List of Tables

Nomenclature

Bragg's angle	θ
X-ray Density	ρ_x
Bulk density	ρ_B
Coercivity	H_C
Grain diameter	D
Direct Current	DC
Alternating current	AC
Sintering Temperature	T_s
Miller indices of the crystal planes	h, k, l
Lattice parameter	a
DC resistivity	ρ_{dc}
Dielectric constant	ϵ'
Frequency	f
Imaginary part of initial permeability	μ''
Impedance	Z
Inductance	L
Initial permeability	μ'
Loss factor	$\tan\delta$
Magnetization	M
Magnetic field	H
Field Effect Scanning electron microscopy	FESEM
Vibrating sample magnetometer	VSM

Nelson-Riley function	$F(\theta)$
Number of turns	N
Boltzmann constant	K_B
Relative quality factor	RQF
Remanent Induction	M_r
Saturation magnetization	M_S
Saturation induction	M_r
Oersted	Oe
X-ray diffraction	XRD

Chapter 1: General Introduction

Modern materials science research is centered on developing novel materials with improved properties and unconventional synthesis methods to meet the rising technological demands in a wide range of sectors. Ferrites' immense usefulness and unique characteristics have made them the subject of intense interest. Owing to their extensive array of technical uses, fixed magnets, magnetic fluids, electromagnetic devices, disk recording, magnetic cooling systems, and high-density storage are just a few examples, ferrites are currently the subject of intense study. In this chapter, we've covered the introduction to ferrites.

1.1. Ferrites

Ferrites, a significant category of minerals with very strong magnetic characteristics, have been researched and used for over five decades owing to their magnetization saturation, enhanced electrical resistivity, diminished electrical losses, and exceptional chemical stability. Ferri-magnetic materials include ferrite, according to Neel [1]. The material in question is a ceramic composite of one or more metallic elements and iron oxide (Fe_2O_3)

constituents. Ferromagnetic materials are characterized by their electrical non-conductivity and ability to become magnetized. The formation of ferrite is through the chemical reaction between the oxide of ferric, commonly known as oxidation, and various metallic elements such as nickel, manganese, zinc, magnesium, aluminum, barium, copper, cobalt, or iron.

The formula $MO.Fe_2O_3$ (Fe_xO_y) is commonly employed in various applications, whereby M represents a divalent cation such as Ni^{2+}, Cu^{2+}, Zn^{2+}, Cd^{2+}, Mn^{2+}, Fe^{2+}, Mg^{2+}, Co^{2+}, or a combination thereof with a valency of two on average. The chemical compositions of

Nickel, Manganese, and Zinc ferrites are denoted as $NiFe_2O_4$, $MnFe_2O_4$, and $ZnFe_2O_4$, respectively. The molecular descriptions of ferrites are able to be expressed in a thorough formula as AB_2O_4, with A and B denoting distinct metal cations.

1.2. History of Ferrites

Ferrites, which are magnetic oxides, have historical roots, may be traced back to antiquity, predating the birth of Christ. During this time, identifying stones that could attract iron marked the initial recognition of this phenomenon. The area of Magnesia in Asia Minor was recognized as the primary location for abundant quantities of these stones, leading to the mineral being named magnetite (Fe_3O_4). The initial systematic investigation of the correlation, magnification, and chemical characteristics of several binary ion oxides was conducted by Hilpert in 1909. The investigation of the correlation among material properties, saturation magnetic field, and melting point was undertaken by Hilpert and Wille in Germany and Forestier in France in about 1928. Kato and Takei are often credited with discovering modern ferrites by examining $CoFe_2O_4$ in the 1930s. Japanese researchers conducted investigations into magnetic oxides between 1932 and 1935. The investigation of magnetic oxides was conducted by Japan's Takei (1939) and the Netherlands' Snoek (1937). At the Philips study labs in the Netherlands, Snoek and his coworkers conducted a study on a significant characteristic of loss factor, defined as the ratio of loss tangent to permeability. This investigation ultimately resulted in Snoek's pioneering work, producing the initial soft ferrites for commercial use. Neel put forth the initial theories elucidating the genesis of magnetism in ferrites in 1948. Guillaud et al. conducted a subsequent investigation into the technology of ferrites. The first soft ferritin release was formally announced in 1969. At that point, ferrites gained recognition as a significant category of magnetic materials [1].

1.3. Types of ferrites

In contemporary times, the term "ferrite" refers to magnetic oxides, mainly composed of iron oxide. Ferrites are categorized according to their crystalline structure, cation distribution, and magnetic characteristics.

Ferrites are frequently categorized as soft or hard according to their magnetic properties, which allude to their moderate or elevated coercivity. Ferrites with dielectric qualities do not naturally conduct electricity, despite the ability of electromagnetic waves to travel through them.

Additionally, because these metals conduct electricity, they often exhibit magnetism, providing them an advantage over Fe, Ni, and other transition metals. Due to the strength of their coercive fields, there are two groups of ferrites.

1.3.1. Soft ferrite

Ferrites with nickel, zinc, and manganese compounds are typically found in the cores of transformers and electromagnetic devices. They are known as soft ferrites due to their low coercivity, which enables them to change the magnetization direction easily using low energy. While eddy currents in the core are eliminated due to high resistivity. The soft ferrites are suitable as the core of RF transformers and inductors because they lose little power at higher frequency regions.

1.3.2. Hard ferrites

On the other hand, ferrite magnets that last a long time are constructed from hard ferrites that retain their magnetism for a long time. The oxides of iron, barium, and strontium make up these. Because of their high coercivity, these materials are excellent examples of permanent magnets since they are highly resistant to demagnetization. They are effective magnetic flux conductors with a high magnetic permeability. Supposed ceramic magnets are able to hold magnetic fields more potent than iron itself. They're inexpensive and found practically everywhere, such as refrigerator magnets.

The range of magnetic field strengths H is around 30–160 kA/m (400–2000 Oersteds), with a maximum of 0.35 tesla for magnetic field B. Around 5 g/cm3 is the density of ferrite magnets.

1.3.3 Kinds of Crystal Structure of Ferrites

The ferrites, consisting mostly of the combination Fe_2O_3, are split into five classes, including the hexagonal or magneto-plumbite ferrites and the cubic, spinel, garnet, and ortho ferrites. Comparing Fe_2O_3 to other oxides by molar ratio found in the ceramic distinguishes these ferrites.

1.3.3.1 Cubic

For cubic ferrites, the usual formula is $MO.Fe_2O_3$, where M is the metal ion of valence 2 (Mn, Cu, Cd, Ni, Fe, Co, Zn, Mg, etc.). Similar to ZnO in zinc ferrite. Magnetically, the softness of all other cubic ferrites is alleged, while Fe_2O_3 is magnetically hard. The cubic ferrites are also termed as ferro-spinel, owing to the similarity in crystal structure to the mineral spinel $MgO.Al_2O_3$. The Mg and Al in ferrites are swapped out for the corresponding divalent and trivalent ions. Substitution ions should always have ionic radii between 0.5 and 1 Å.

1.3.3.2 Spinel

The formula AB_2O_4 represents the spinel ferrites, where A is the metal ion of valence two and B is iron. Although spinel ferrites may be used in place of metallic magnets like iron and layered iron-silicate alloys because of their soft magnetic qualities, their enhanced magnetic properties enable them to function even better [2, 3]. Minimal magnetic losses and high electrical resistance are two of the characteristics of spinel ferrites. Spinel ferrite is a family of ceramic magnets that includes the well-known Ni-Zn and Mn-Zn ferrites, as well as the less common cobalt zinc and others. Their high permeability to magnetic fields and electrical resistivity, and potential for modifying

intrinsic properties across a broad spectrum, have made them fascinating ceramic materials [4].

1.3.3.3 Garnet

The garnet-type ferrites are a different class of ferrites. Garnets, a particular type of magnetic ceramic, are employed in magneto-optical applications because of their optical transparency [5]. Yttrium iron garnets (YIG) are synthetic garnets with the chemical formula $Y_3Fe_5O_{12}$. One of the ions of rare earth with an atomic number larger than 61, such as La^{3+}, Dy^{3+}, Gd^{3+}, and Er^{3+}, can replace yttrium.

1.3.3.4 Ortho Ferrites

Because they are extraordinarily fast, domain wall motion speeds, ortho ferrites are employed in optical internet, monitors for fields of magnetic resonance and currents of electricity, mechanical measurements, and other areas.

1.3.3.5 Hexagonal

Permanent magnetic properties were discovered in 1952 in a group of ferrites that had been previously unknown. In Eindhoven, the Netherlands, employees of the Philips laboratory developed hexagonal ferrites. The high uniaxial magneto-crystalline anisotropy of the common formula for hexagonal ferrites is $MFe_{12}O_{19}$, where M is usually either lead (Pb), calcium (Ca), strontium (Sr), or barium (Ba), making them ideal for use as permanent (hard) magnets [6]. Hexaferrite has a complicated crystal structure, yet its basic hexagonal shape and single *c*-axis make magnetization relatively simple. Due to the difficulty in switching the magnetic orientation of hexagonal ferrites, the term "hard" is often used to describe these materials. Recently, much attention has been paid to hexagonal ferrites, such as strontium ferrite ($SrFe_{12}O_{19}$) and barium ferrite ($BaFe_{12}O_{19}$), which are used in microwave devices. Because of its incredible resistance and strong uniaxial anisotropy, barium hexaferrite is a possible substitute for yttrium iron garnet [7] in microwave integrated circuits and devices. Performing superior to

existing devices, planar, self-biased, and low-loss, microwave magnetic devices that are planned to be developed in the future will have circulators, phase shifters, filters, isolators, and other related components [8].

1.3.4 Classification of Spinel Ferrites by Cation Distribution

In general, spinel ferrites have the following chemical formula: MFe_2O_4, where M is any metal ion that is divalent, including Ni^{2+}, Mn^{2+}, Co^{2+}, Zn^{2+}, Fe^{2+}, Mg^{2+}, Cd^{2+}, or any of these ions in combination. Spinel is a mixed metal oxide, which is a large group of substances that all have the same chemical formula $A^{2+}B^{3+}O_4^{2-}$. Typically, A is a trivalent metal like Ti, Fe, Al, and Co, and B metals, such as Mg, Mn, Fe, Zn, and others, are divalent. 32 oxide ions are arranged in a cubic closed-packed array to create 64 tetrahedral (A-sites) holes and 32 octahedra (B-sites) in each unit cell. Spinel comes in three primary varieties [9, 10]:

- Normal spinel structure: $\delta = 1$
- Inverse spinel structure: $\delta = 0$
- Mixed spinel structure: $0 < \delta < 1$.

1.3.4.1 Normal Spinel Ferrites

In this class, all of the Me^{2+} ions occupy the A positions; 16 trivalent cations occupy 16 B sites, while 8 divalent cations occupy 8 A-sites. $Me^{2+}\ [Fe_2^{3+}]\ O_4^{2-}$ is the structural formula for such ferrites. This category includes the zinc ferrites, $Zn^{2+}\ [Fe^{2+}Fe^{3+}]\ O_4^{2-}$. Fig. 1.1 depicts the common spinel ferrites.

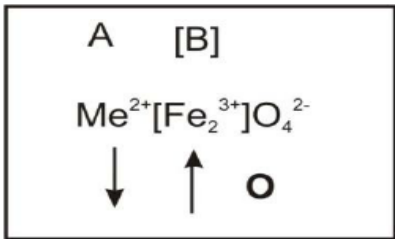

Fig.1.1: Normal Spinel ferrites.

1.3.4.2 Inverse Spinel Ferrites

Inverse spinel ferrites have tetrahedral and octahedral sites with equal distributions of Fe^{3+} ions; all Me^{2+} ions are found in octahedral locations. Fe^{3+} $[Me^{2+}$ $Fe^{3+}]$ O_4^{2-} is the structural formula for these ferrites. The spinel structures Fe_3O_4, $NiFe_2O_4$, and $CoFe_2O_4$ are inverted. Figure 1.2 depicts an inverse spinel ferrite.

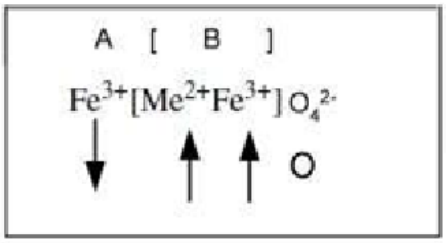

Fig. 1.2: Inverse Spinel ferrites.

1.3.4.3 Mixed Spinel Ferrites

Different types of spinel are called "mixed spinel" if the Me^{2+} cations are spread out in both tetrahedral and octahedral places. The chemical formula of these ferrites is $Me_{1-\delta}^{2+}$ Fe_{δ}^{3+} $[Me_{\delta}^{2+}$ $Fe_{2-\delta}^{3+}]$ O_4. Fig. 1.3 depicts a mixed spinel ferrite.

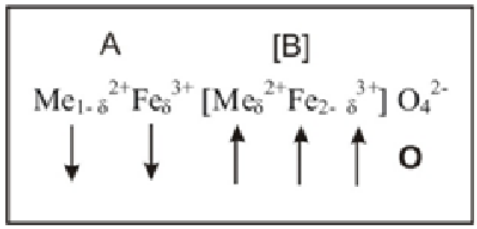

Fig. 1.3: Mixed Spinel ferrites.

1.4. Applications of Ferrites

Ferrites find utility in a variety of applications, which include:

- Due to their increased resistance, lower cost, easier production process, and improved magnetization properties, ferrites are considered preferable magnetic materials when compared to pure metals.

- The main applications for ferrites are as inductive parts in filters, voltage-controlled oscillators, impedance-matching networks, low-noise amplifiers, etc.
- The use of magnetic materials at high frequencies as the building blocks of power transformers in radar, electronic, and communications systems.
- Ferrites are commonly employed as coil cores owing to lower eddy current losses in computer memory core components and microwave frequency devices.
- Ferrites are considered inappropriate for applications requiring strong fields with powerful equipment, including power transformers, generators, and motors, since their flux density and permeability are quite low. However, they can find utility in applications requiring low power and a low field.
- In electrical circuits, ferromagnetic insulators are frequently employed utilizing ferrites.
- Ferrites, such as ZnO, are utilized in applications of frequencies below a certain level concerning schedules. Additionally, as switches in they are used in various appliances such as refrigerators and AC systems.
- Ferrites are commonly employed as magnetic head transducers in recording applications.

1.5 Overview of the present compound and motivation

Ni-Zn and Mn-Zn ferrites, which are also referred to as Zn-substituted Ni and Mn ferrites, are the most significant commercial forms of these ferrites. Their resistivity levels are the main way that these two types of ferrites differ from one another. The high magnetization and permeability of Mn-Zn ferrites make them significant from a technological standpoint. Their low resistivity, however, causes their loss of eddy current to increase at higher frequencies. Transformer coils and recording heads are just

a few of the electronic components that are used a lot by these ferrites. Conversely, Ni-Zn ferrites have elevated resistivity but reduced permeability at high frequencies. Phase shifters, propagators, insulators, capacitors, and inverters are examples of the numerous devices and electrical components that use these ferrites as their magnetic core materials. For magnetic materials to be used in high-frequency pulse transformers and computer memory, they must have high saturation magnetization, minimal magnetic losses, a high Neel temperature, and enormous resistivity. Despite much research on Mn-Zn and Ni-Zn ferrites individually, there is a noticeable lack of coverage when it comes to ferrites together. Impurities change the crystal's shape and flawed structure when they are present [11], significantly altering the materials' magnetic and electrical properties. The impact of Cr^{3+} substitution inside the spinel framework of ferrites was investigated by several researchers [12–18]. From an application standpoint, Mn-Zn and Ni-Zn ferrites are particularly significant because they are employed in a variety of ferrite devices, such as electromagnetic wave absorbers, magnetic heads, converters, and inductor cores [19]. A group of Ni-Zn ferrites replaced with Cr made using the oxalate decomposition method was described by A.M. EI-Sayed et al [18]. The A site in the AB_2O_4 crystal structure is tetrahedral, whereas the B site is octahedral. Neel's two-lattice model successfully explains how saturation magnetization (M_s) declines as Cr ions increase. Additionally, it was believed that a reduction in conductivity with increased Cr concentration resulted from the referential occupancy of Cr^{3+} ions by octahedral sites, which substituted Fe^{3+} ions and hindered Fe^{2+}-Fe^{3+} conduction. However, we could not locate any reports on the Cr^{3+}-substituted Ni-Mn-Zn ferrite in the literature. As a result, we aim to synthesize the $Ni_{0.6}Mn_{0.2}Zn_{0.2}Cr_xFe_{2-x}O_4$ ferrites (x = 0.0, 0.05, 0.10, 0.15, and 0.20) by the solid-state reaction (SSR) technique and characterization.

Motivation

The commercial significance of polycrystalline ferrite is widely acknowledged. Hence, the research interest in these materials is always inspiring. The factors that can effectively alter the characteristics of ferrites include the preparation process, composition, replacement, sintering heat, sintering duration, and sintering rate [20]. To facilitate technological applications, it is essential to identify and devise strategies for investigating and enhancing the properties of these materials under appropriate conditions. Despite the existence of a considerable body of literature on Ni-Mn-Zn ferrites, currently, there are no studies examining the impact of Cr^{3+} ion replacement on the $Ni_{0.6}Mn_{0.2}Zn_{0.2}Fe_2O_4$ ferrites prepared by the double sintering method. The Cr^{3+} ion has been substituted in other ferrite systems, where a significant effect of Cr^{3+} ion substitution is observed [mentioned above]. Thus, we have selected the Cr^{3+} ion as a substitute ion. In this study, the objective is to synthesize $Ni_{0.6}Mn_{0.2}Zn_{0.2}Cr_xFe_{2-x}O_4$ ferrites (where x = 0.0, 0.05, 0.10, 0.15, and 0.20) utilizing the two-step annealing procedure. The aim was to examine the changes in structural, morphological, electrical, and magnetic properties resulting from the substitution of Cr^{3+} in the Ni-Mn-Zn ferrites.

1.6 Objectives with Specific Aims

Combining $Ni_{0.6}Mn_{0.2}Zn_{0.2}Cr_xFe_{2-x}O_4$ ferrites (where x = 0.0, 0.05, 0.10, 0.15, and 0.20) by an SSR approach and characterizing their structural, electrical, and magnetic characteristics are the main goals of the present work.

The following are the goals of this thesis:

- Synthesis of $Ni_{0.6}Mn_{0.2}Zn_{0.2}Cr_xFe_{2-x}O_4$ ferrites with x values of 0.00, 0.05, 0.10, 0.15, and 0.20.
- Examining the structural characteristics using the X-ray diffraction (XRD) method.
- Studying the shape of the made samples' surfaces using a scanning electron microscope (SEM).

- The samples will have their magnetic properties checked using the vibrating sample magnetometer (VSM), which includes measuring their magnetization, M-H loop, and saturation magnetization.
- An impedance analyzer will be used to examine the A.C. electrical transport characteristics, particularly the complex impedance spectra, A.C. electrical resistivity, and dielectric constants.

1.7 Arrangement of the Thesis

The following is an outline of the six chapters that make up the thesis:

Chapter 1 # General Introduction

This chapter presents an overview of Ni-Mn-Zn ferrites and outlines the thesis structure. It also covers the classification of ferrites, recent reports, and the background material necessary to understand the investigation's goals and objectives.

Chapter 2 # Literature Review

This chapter presents a review of the Ni-Mn-Zn, doped Ni-Mn-Zn, and Cr-doped ferrites.

Chapter 3 # Materials and Methods

The methods for sample preparation and characterization are covered in Chapter Three. The sample preparation and data acquisition techniques are elaborately discussed in the Chapter.

Chapter 4 # Results and Discussion

The obtained results are presented in Chapter 4 and discussed with proper formalism.

Chapter 5# Conclusions

This chapter provides a summary of the study's findings.

References

[1] J.M.D. Coey, Magnetism and Magnetic Materials.

[2] E. C. Snelling, "Soft Ferrites: Properties and Applications", 1st Edition, Iliffe Books Ltd., London, 1969.

[3] M. Sugimoto, Journal of American Ceramic Society, 82 (1999), 2, 269.

[4] L. L. Hench, J. K. West, "Principles of Electronic Ceramics", John Wiley & Sons, 1990.

[5] A. J. Moulson, J. M. Herbert, "Electro-ceramics: Materials, Properties, Applications", 1st Edition, Chapman & Hall, London, 1990.

[6] A. L. Stuijts, G. W. Rathenau, G. H. Weber, Philips Technical Review. 16 (1954), 141.

[7] H.C. Fang, C.K. Ong, Journal of Applied Physics, 86 (1999), 2191.

[8] H. W. Gorter, Philips Research Reports. 9 (1954), 295.

[9] Harris, V. G. Chen, Z. Chen, Y. Yoon, S. Sakai, T. Gieler, A. Yang, A. He, Y. Ziemer, K. S. Sun, N. X. Vittoria, Carmine, Journal of Applied Physics. 99 (2006), 911.

[10] M. G. Naseri and E. B. Saion, Crystallization in spinel ferrite nanoparticles, www.intechopen.com, 2012, 352-353.

[11] A.M. Sankpal S.S. Suryavanshi, S.V. Kakatkar, G.G. Tengshe, R.S . Patil, N.D. Chaudhari, S.R. Sawant, J. Magan. Mater. 186(1998), 349-356.

[12] A.M. EI-Sayed, Ceramics International. 28 (2002), 651-655.

[13] A.M. EI-Sayed, Materials Chemistry and Physics. 82 (2003), 583.

[14] S.M. Patange, S.E. Shirsath, B.G. Toksha, S.S. Jadhav, K.M. Jadhav, Journal of Applied Physics. 106 (2009), 023914.

[15] D.R. Mane, Swati Patil, D.D. Birajdar, A.B. Kadam, S.E. Shirsath, R.H. Kadam, Materials Chemistry and Physics. 126 (2011), 755.

[16] A.A. Birajdar, S.E. Shirsath, R.H. Kadam, S. M. Patange, K.S. Lohar, D.R. Mane, A.R. Shitre, Journal of alloys and compounds. 512 (2012), 316-322.

[17] M.A. Gabal, Y.M. Al Angari, F.A. Al-Agel, Journal of Magnetism and Magnetic Materials. 391 (2015), 108-115.

[18] F. Alam, B.C. Das, A. K. M. A. Hossain, Proceedings of 14th Global Engineering and Technology Conference, 29-30 December 3017, BIAM Foundation,63 Eskaton, Dhaka, Bangladesh.

[19] F. Alam, M.L. Rahman, M.H.R. Khan, A.K.M.A. Hossain, Journal of Modern Physics. 5 (2014), 1223-1233.

[20] D.C. Sinclair, A.R. West, Journal of Applied Physics. 66 (1989), 3850.

Chapter 2: Literature Review

The parent composition considered here has already been studied by different research groups at home and abroad due to its potential application in diverse fields of applications. On the other hand, Cr has also been substituted in many ferrite compositions owing to its significant impact on the dimensions of the ferrites. Thus, some of the reports on Ni-Mn-Zn ferrites and Cr^{3+} doped ferrites have been presented in this chapter.

2.1 Literature Review of Ni-Mn-Zn Ferrite

Amarendra et al. [1] investigated the electrical characteristics of ferrites produced using the citrate precursor technique that was Mn-substituted with $Mn_xNi_{0.5-x}Zn_{0.5}Fe_2O_4$, where x ranges from 0.05 to 0.4, and show how these characteristics changed with frequency, conditions, structure, and annealing temperature. For each sample, up to 1 kHz, the dielectric constant exhibits a rapid decrease, followed by a slight decline between 1 and 10 kHz, and remains almost steady beyond 10 kHz. This dispersion of the electrical strength is attributed to hopping conduction among Fe^{3+} and Fe^{2+}, Mn^{2+} and Mn^{3+}, and Ni^{2+} and Ni^{3+} ions. Furthermore, the observation was made that the dielectric property increases with increasing concentration of Mn, except for sample x=0.3, which displayed a rapid decrease.

V. More et al. [2] analyzed the impact of Ce^{3+} substitution regarding the characteristics of Ni-Mn-Zn ferrites nanoparticles, wherein the components are obtained using the sol-gel auto-combustion (SGAC) technique. The correlation between the constant of the

dielectric and the applied frequency was demonstrated within the spectrum range of 50 Hz to 5 MHz. The researchers investigated the characteristic behavior shown by spinel ferrites, wherein the dielectric constants demonstrate a notable increase at lower frequencies, followed by a rapid decline, ultimately reaching a state of near-constancy in the higher frequency ranges. The observed fluctuation in the real component of permittivity was elucidated by considering atomic, electronic, ionic, and interfacial polarization mechanisms [3]. Koop's phenomenological theory served as the foundation for the Maxwell-Wagner model, which was used to characterize the frequency response of grains and grain boundaries [4-7]. A low-loss dielectric behavior due to higher resistivity [7] is advantageous for high-frequency data storage applications.

N. Khatun et al. [8, 9] studied the microstructure of $Ni_{0.08}Mn_{0.90}Zn_{0.02}Fe_2O_4$ ferrites using SEM, and the typical size of the grain, as calculated from the resulting micrographs, is between 0.27 μm to 0.88 μm. Grain clustering appears to have begun at about 1050°C, while the development of acute notch-type grains occurred between 1100°C and 1150°C. The dimension of grains was also observed to expand with the degree of sintering. All samples exhibited typical ferromagnetic behavior, with dielectric constants (έ) decreasing as frequency increased. Koop's theory and polarization of the Maxwell-Wagner type may account for this occurrence. [10, 11].

The study by Zhong et al. [12] explored the effect of NiO on the magnetic properties and microscopic structure of $Zn_{0.32}Mn_{0.60-x}Ni_xFe_{2.08}O_4$ ferrites. Adding Ni decreased the lattice constant, grain size, and porosity, and increased the grain structure compactness.

H. Begum et al. [13] studied frequency-dependent properties of dielectric constants (έ) of Ni-Mn-Zn ferrites under ambient conditions. The researchers demonstrated the correlation between the dielectric constant and frequency variation. The magnitude of the variable έ exhibited a consistent decline as the frequency increased. Ni-Mn-Zn ferrite samples were found to behave like standard dielectrics in terms of how they

changed with frequency, consistent with the findings reported by Radha and Ravinder [14]. The decrease in electronic exchange between $Fe^{2+} \leftrightarrow Fe^{+3}$ ions is observed when the externally applied electric field exceeds a specific frequency [15]. Ferrites' conduction mechanism is similar to dielectric properties [16, 17]. Additionally, the dielectric loss was observed to diminish when the submitted alternating current (AC) field of charge frequency fell below the variation in the frequency of charges regarding Fe^{2+} and Fe^{3+} ions located at adjacent points of the octahedral. At high applied electric field frequencies, the electron exchange hopping frequency has a limited ability to track the applied field above an essential frequency with minimal reduction. The highest tanδ was seen at 10 MHz. The phase angle tangent (tanδ) exhibited a progressive decline as the frequency increased.

The researchers observed the fluctuation of initial permeability in connection with vibration for specimens that underwent grinding at a temperature of 1100°C. The value of μ_i exhibited an upward trend as the Ni concentration increased, owing to the concurrent rise in particle size and magnetization enhancement [18]. The frequency had an impact on the initial permeability of the sample. Therefore, it is possible to achieve a higher initial permeability by increasing the nickel concentration. Nevertheless, this augmentation in permeability is correlated with a reduction in frequency stability. Furthermore, it was observed that the permeability exhibited a significant drop in regions characterized by low frequencies, ultimately reaching a state of near-constant values. The permeability of ferrites is linked to two distinct phenomena, specifically, the magnetization of spin rotation inside the domains and the mobility of domain barriers [19–20]. The Q value of Ni-Mn-Zn ferrites exhibits a progressive increment when the frequency is raised. Ferrites demonstrate a high Q-factor and direct current resistivity on the order of 10^6 Ω-cm, making them highly advantageous for transformer core applications within the range of a few MHz frequencies.

S. Ramesh et al. [21] studied the $Ni_{0.4}Zn_{0.6-x}Mn_xFe_2O_4$ systems, examining the relationship between the lattice constants and the manganese (Mn) contents. A decline in the lattice constant was observed up to x = 0.15, which is increased with a further increase in Mn concentration. They investigated the magnetic properties of $Ni_{0.4}Zn_{0.6-x}Mn_xFe_2O_4$ ferrite nanoparticles utilizing a VSM at room temperature within an external magnetic field range of ±11 kOe. All the samples have reached magnetic saturation, indicating ferrimagnetic characteristics of Ni-Zn-Mn nanoparticles, as evidenced by their finite coercivity values. The M_s and coercivity (H_c) were determined from the M-H loops, and their changes were analyzed for different Mn contents.

The study was conducted by Eltabey et al. [19] on the correlation between the concentration of Nd^{3+} ions and the initial permeability (μ_i) of $Mn_{0.5}Ni_{0.1}Zn_{0.4}Nd_xFe_{2-x}O_4$ ferrite samples at ambient temperature. As the concentration of Nd rises, the value of μ_i shows an increasing trend. Images from SEM demonstrated that the typical grain size, denoted as D, has relatively little dependence on neodymium (Nd), represented by x. Furthermore, the augmentation of x reduces the concentration of iron ions within the ferrite molecule. The presence of Fe^{2+} ions is widely recognized as the primary cause of anisotropy in ferrites [20]. Therefore, the anisotropy constant k_1 exhibits a decrease. When the value of k_1 decreases, μ_i increases as per the Globus relation. In addition, substituting Nd^{3+} ions contributes to the enhancement of M_s, leading to a rise in μ_i for the samples within the range of $0 \leq x < 0.05$.

D. R. Mane et al. [22] employed an SGAC approach to synthesize $Ni_{0.7-x}Mn_xZn_{0.3}Fe_2O_4$ ferrites, where the value of x was incremented by 0.1 from 0.0 to 0.7. The synthesis process involved the utilization of nitrates of the corresponding metal ions. These results show that Mn substitution had a significant impact on the combustion response as well as the properties of the Ni–Zn ferrite powder. Until x = 0.2, M_s increases with the increase in Mn concentration, and then it gradually decreases.

The research undertaken by U.B. Gawas et al. [23] studied the effect of the melting point on electrical properties, microstructure, and initial permeability of $Ni_{0.5-x}Mn_xZn_{0.5}Fe_2O_4$ ($0.0 < x < 0.5$) samples generated by the initial combustion process. The structure with x = 0.2 consumed at 1200 °C has the highest initial permeation value of 621.3. To be used in electromagnetic appliances, ferrites must have minimal dielectric losses, superior resistivity, and high initial permeability.

In a study by F. A. Ahmed et al. [24] synthesized the $Mn_{0.5-x}Ni_xZn_{0.5}Fe_2O_4$ (x = 0.0, 0.1, 0.2, and 0.3) ferrites through a SGAC and analyzed the dimensional and metallic behavior of the nanostructures. The highest M_s peak is observed for x=0.1 and diminishes as the level of Ni replacement increases.

High-density magnetic recording materials, Ni^{2+} and Co^{2+} substituted Mn-Zn ferrites, have been examined by Babbar et al. [25]. $Mn_{o.6}Zn_{o.4-x}Ni_xFe_20_4$ and $Mn_{o.6}Zn_{o.4-y}Co_yFe_20_4$ ferrite series were synthesized via hot pressing with x and y varying from 0 to 0.4 in 0.05 increments. Researchers have studied the effects of different concentrations of Ni^{2+} and Co^{2+} ions on a material's electrical resistivity and coercive field. The study also suggests that replacing some Zn^{2+} ions with Ni^{2+} or Co^{2+} ions enhances the magnetic properties without significantly altering the material's microstructural features. These ferrites can potentially be useful in developing powerful magnets for incredibly dense magnetic recording due to their low porosity, small grain size, and high initial permeability at high frequencies.

The $Mn_{0.5}Ni_{0.1}Zn_{0.4}Al_xFe_{2-x}O_4$ (x=0 to x=0.15, in a step of 0.025) ferrites, synthesized using a normal ceramic process, have had the effect of Al-doping on their magnetic properties, IR spectra, and physical characteristics investigated by A.A. Sattar et al. [26]. In Mn-Ni-Zn ferrites, they discovered that replacing Al-ions reduced the lattice parameter and increased porosity. The Mn-Ni-Zn ferrites that were replaced in all of the

samples showed elevated Curie temperatures and DC resistivity. High-frequency applications show potential for the results.

The study by S. Ramesh et al. [27] examined Ni-Zn ferrite systems by systematically substituting Mn [$Ni_{0.4}Zn_{0.6-x}Mn_xFe_2O_4$, x = 0.00 to 0.25], prepared using the SGAC process. The resistivity of the Ni-Zn-Mn combination exhibits an initial increase as the concentration of Mn is varied.

Applying the SGAC technique, J. Pei. et al. [28] synthesized Ni-Mn-Zn ferrites doped with Mo^{6+} - [$Ni_{0.5}Zn_{0.5}Mn_{0.5-x}Mo_xFe_{1.5}O_4$ (x = 0.025, 0.05, 0.075, and 0.1)], which were further studied by VSM, FESEM, FTIR, and X-ray diffraction (XRD) measurement. The doping of Mo^{6+} ions considerably influences ferrites' microstructure and soft magnetic characteristics. As the magneto-crystalline anisotropy constant dropped, from 67.3 to 12.1 Oe, the H_c dropped, while the M_s increased.

More et al. [29] prepared $Ni_{0.35}Mn_{0.35}Zn_{0.3}Fe_{2-x}Ce_xO_4$ (x = 0.0, 0.025, 0.050, 0.075, and 0.1) ferrite nanoparticles by the SGAC method, which were characterized using XRD, SEM, EDAX, VSM, and dielectric measurements. Magnetic properties of Ni-Mn-Zn soft ferrites substituted with Ce^{3+} and sintered at 9000°C. In the Ni-Mn-Zn crystal lattice, the M_s rises linearly when Fe^{3+} ions are substituted by Ce^{3+} ions at the octahedral B site. They found that M_s rises from 64.42 to 72.04 emu/gm.

The $Ni_{0.4}Zn_{0.6-x}Co_xFe_2O_4$ and $Ni_{0.4}Zn_{0.6-x}Mn_xFe_2O_4$ (x = 0.00 to 0.25) were investigated by S. Ramesh et al. [30]. The study also shows the magnetic properties of both bulk and nano Ni–Zn–Mn and Ni–Zn–Co ferrites, along with their corresponding crystallite/grain sizes, to help understand how replacing Mn/Co affects the Ni–Zn ferrites. The *M*s of the Ni–Zn–Mn system vary from 66 to 89 emu/g, whereas those of the Ni–Zn–Co system range from 61 to 91 emu/g. This indicates that the Mn/Co replacements resulted in

greater magnetization values than the nano forms. The bulk material shows a slight increase in M_s values compared to its nanocrystalline versions.

2.2 Literature Review of Chromium-Doped Ferrite

Shinde et al. [31] have studied $Ni_{0.2}Cu_{0.2}Zn_{0.6}Fe_{2-x}Cr_xO_4$, ($x$ = 0.0, 0.05, 0.10, 0.15, and 1.20) ferrites, which were prepared using the SGAC process. The researchers have documented the impact of substituting Cr ions on porosity, resulting in a rise from 25.4% to 32%. In the series, it has been noted that as the Cr^{3+} substitution rises, the unit cell's volume and molecular weight decrease. The researchers discovered that the observed rise in porosity can be primarily attributable to the concurrent drop in the size of the crystallite. This reduction in size leads to an increase in grain boundaries within the particle, thereby increasing porosity [32].

Hashim et al. [33] have conducted a study in which they successfully synthesized nanoparticles of $Ni_{0.5}Mg_{0.5}Fe_{2-x}$ Cr_xO_4 ($0 \leq x \leq 1.0$) using the SGAC method. After synthesizing the nanoparticles, the researchers studied their dielectric and magnetic characteristics [34]. When Cr^{3+} ions were introduced by doping in Mg-Cr ferrites, the M_s decreased to 1.546 emu/g from 11.08 emu/g. As Cr^{3+} concentration rose, the H_c decreased from 97.06 Oe to 19.02 Oe. This phenomenon may be explained by the decrease in the anisotropy field, which lowers the domain wall energy [1].

The Mn-Zn ferrites with Cr^{3+} substitution ($Mn_{0.50}Zn_{0.50}Cr_xFe_{2-x}O_4$, where x takes values of 0.00, 0.1, 0.2, 0.3, 0.4, and 0.5) were produced through the combustion process [35]. The results obtained from the concentration range examined demonstrate a decline, and the saturation magnetization has an increased amount of paramagnetic Cr^{3+}. As saturation magnetization decreases, it can be attributed to a gradual reduction in the number of

Fe^{3+} ions present at B sites. This reduction ultimately causes a decrease in the magnetization of the B sublattice. The ferrites of Mn-Zn-Cr [36] and Mg-Mn-Cr [37] also showed a similar decline.

Pankaj et al. [38] used the SSR method to prepare Cr-doped Mn-Zn ferrites [$Mn_{0.5}Zn_{0.5-x}Cr_xFe_2O_4$ (x=0.00, 0.30, 0.50)]. The researchers observed a decline in the ε′ with increasing frequency and noted that it reached a minimum (constant) value at higher frequencies. The observed reduction in the ε′ with frequency may be attributed to electron hopping between Fe^{2+} and Fe^{3+} ions, which hinders their response to the applied electric field. The phenomenon of a reduction in ε′ as frequency increases has been previously discovered for Ni-Zn ferrites [39]. The observed drop in the ε′ with frequency is a characteristic dielectric nature commonly found in spinel ferrites. This phenomenon can be attributed to dipole relaxation.

Praveena et al. [40] investigated the relationship between magnetization and applied magnetic field for $Ni_{0.4}Zn_{0.2}Mn_{0.4}Fe_2O_4$ ferrite powders that have been sintered at various temperatures. The authors analyze the hysteresis loop to examine this relationship. The loops demonstrate characteristics of both low power loss and low coercivity. The saturation magnetization values increased from 23.91 to 55.80 Am^2/kg due to the sintering process conducted at temperatures ranging from 400 to 700 ^oC for 4 hours. Similarly, the coercive field experienced a transition from 4.79 to 6.39 kA/m. As the sintering temperature increases, the squareness factor (M_r/M_s) exhibits a monotonically rising trend. The average grain size of $Mn_{0.50}Zn_{0.50}Cr_xFe_{2-x}O_4$ ferrite samples is determined by observing their surface morphology in a high-resolution optical microscope [41]. Grain sizes typically range from 3.4 μm to 5.7 μm on average. Sintering at higher temperatures results in larger grains. This is because the pore volume is reduced, and the grain size is increased because the grain boundaries are driven to develop across the pores by the heat energy generated during the sintering process.

In their study, F. Alam et al. [35] examined the relationship between magnetization (M) and applied magnetic field (H) for different compositions of $Mn_{0.50}Zn_{0.50}Cr_xFe_{2-x}O_4$ (with x=0.0 to 0.5). The measurements were conducted at 300 K. The researchers observed that the magnetization of all samples exhibited a linear relationship with the applied magnetic field, increasing up to 0.1 T. In the realm of this particular applied field, the phenomenon of magnetization exhibits a gradual growth, eventually reaching a state of saturation. The magnetization curve is extrapolated to $\mu_0 H = 0$ to find the M_s, for each sample. The researchers noted a decrease in M_s when the Cr^{3+} content increased within the examined range.

In a study, Rintu et al. [42] reported a correlation between frequency and AC conductivity in the ferrite composition $ZnCr_xFe_{2-x}O_4$ (with x=0.0, 0.2, 0.4, 0.6, 0.8, 1.0). This phenomenon can be attributed to employing the two-layer model of Maxwell-Wagner in polycrystalline ferrite. It was observed that AC conductivity exhibits an upward trend as the concentration of chromium ions is increased. The phenomenon of AC conductivity is initially observed to show a positive correlation with frequency, increasing its value. Subsequently, it reaches a peak value, demonstrating a decreasing trend. As the applied field's frequency rises, the ability of charge carriers to hop in response to the applied field diminishes, reducing the values of alternating current (AC) conductivity. The researchers also studied the surface morphology of the ferrite samples using SEM, which demonstrates a lessening in grain size with higher Cr content.

M. Raghasudha et al. [43] performed the study to show the effect of Cr in $MgCr_xFe_{2-x}O_4$ ($0.0 \leq x \leq 1.0$). The H_c decreased from 97.06 Oe to 19.02 Oe as the concentration of Cr^{3+} increased, assumed due to the reduction in the anisotropy field, resulting in a decrease in domain wall energy. It was noticed that an increase in the contents of Cr^{3+} leads to smaller values of the magnetic moment. The researchers demonstrated a negative correlation between the concentration of Cr^{3+} and the anisotropy constant K_i. A decrease

in the K_i constant was observed when substituting the Cr^{3+} ion [44]. The observed phenomenon can be related to the disparity in the ionic radii of the Cr^{3+} ion (0.63 Å) and the Fe^{3+} ion (0.67 Å).

Compared to chromium-substituted mixed Mg-Cd ferrites, the dielectric constant was greater in chromium-substituted cadmium ferrites, as observed in a study conducted by S.A. Masti et al. [45]. The decrease in the dielectric constant in Mg-Cd ferrites containing Cr^{3+} can be attributed to the concurrent rise in resistivity associated with incorporating Cr^{3+} ions in these ferrites.

Baykal et al. [46] presented the M-H curve of $NiCr_xFe_{2-x}O_4$ ($0 < x \leq 1$) at ambient temperature. The decrease in *M*s and magnetic moment is readily seen with increasing Cr^{3+} content. The A site accommodates a portion of the Fe^{3+} ions and Ni^{2+} ions, while the remaining half of the Fe^{3+} ions prefer the B site.

Senbeto et al. [47] performed FTIR studies of $Ni_{0.5}Co_{0.5}Cr_xFe_{2-x}O_4$ ($x = 0$, 0.1, 0.2) ferrites. These measurements were performed in the range of 4,000 to 400 cm^{-1}. Two significant bands of absorption can be seen in the spectra at wave numbers below 1,000 cm^{-1}; these are characteristic features of ferrites. There is a lower-frequency band located between 407 - 424 cm^{-1} and a high-frequency absorption band between 547 - 588 cm^{-1}. The acquired result is consistent with the findings reported in a prior study [48]. This observation aligns with the prepared sample's phase stability and bond formation [49, 50]. This study shows that when the concentration of the Cr^{3+} ion increases for the two frequencies, the absorption band zones shift towards higher wave numbers. FTIR spectroscopy enabled the observation of variations in the emission band.

K. Huang et al. [51] synthesized Cr-substituted Ni-Cu-Zn using an SSR approach (sintered at 1150°C). The ferrites were studied using XRD, revealing single spinel ferrite structures. The diffraction peak slightly shifts towards higher angles upon introducing Cr replacement. Based on the analysis of site preference energies of ions, it is seen that

Cr^{3+} ions exhibit a pronounced inclination towards occupying B sites, resulting in the displacement of Fe^{3+} ions from B sites. The researchers also observed the impact of chromium substitution on the resistivity ρ. The densities of all the samples exhibit a range between 4.95 and 4.80 g/cm^3. The overall trend in density change is decreasing, with a modest rise observed between x = 0.25 and 0.5. The difference between the atomic weights of the original and substituted cations, Cr^{3+} (51.99 amu) < Fe^{3+} (55.85 amu), is what causes the increase in ρ. The observed density reduction could be attributed to intergranular or intragranular factors. Lange and Kellet [52] have established a tight relationship between densification and grain growth. Since each sample's molecular weight greatly lowers when Cr content is added, ρ drops as Cr concentration increases.

A set of nano-crystalline ferrite powder samples, consisting of $CoCr_xFe_{2-x}O_4$, were prepared by M. Azim et al. [53], with varying levels of Cr substitution (x = 0.0 to 0.10, with an increment of 0.02). A rising trend in the lattice constant and unit cell volume of the samples is observed with increasing Cr^{3+} levels. This phenomenon is explained by differences in the elements' ionic radii. The lattice constant a in the sample of pure cobalt ferrite was measured to be 8.3659 Å. The unit cell volume and lattice constant comparative graph shows a rising pattern corresponding to Cr^{3+} content. Moreover, determining the crystallite size was done by the equation $D = k \lambda / B(hkl) \cos\theta$, where the high-intensity peak (311) is employed. The pure sample (x = 0.00) exhibits a crystallite size of 52.2 nm. However, as the Cr^{3+} substitution increases, the crystallite size reduces due to the inhibitory effect of the substituent ions on grain formation. Additionally, it has been noticed that the size of the crystallites falls within the range of 31.5-70.4 nm. The samples at x = 0.00 and 0.02 are suitable for attaining a desirable signal-to-noise ratio on high-density recording medium since their crystallite diameters are < 50 nm [54]. The formula employed to determine the density of X-rays ($\rho_{X\text{-ray}}$) of all

the samples is ρ_{X-ray}= Z M /N_A V. Molar mass differences between Cobalt (58.93 amu), Chromium (52.00 amu), and iron (55.85 amu) are reflected in the X-ray density of produced materials, showing an increasing trend with increases in the substituent ions.

Haque et al. [55] synthesized Cr^{3+}-substituted Mn-Ni-Zn ferrites and studied the structural, dielectric, magnetic, and impedance spectroscopy analysis. For instance, it was noticed that the T_C decreases with the amount of Cr in the composition because Cr has a smaller ionic radius than Fe.

M. Saleem et al. [56] synthesized the $Mn_{0.5}Zn_{0.5-x}Cr_xFe_2O_4$ (x = 0.0, 0.1, 0.2, and 0.5) via the SGAC method. They studied the structural and vibrational characteristics of Mn-Zn ferrites, which revealed a reduction in the lattice constant as the Cr content increases, accompanied by a drop in crystallite size.

As seen in the above literature, the characteristic properties of Ni-Mn-Zn ferrites have made them potential candidates for numerous applications, leading to extensive research on them. We found that Cr^{3+} is substituted in various ferrite compositions, leading to significant magnetic and electrical properties variations. Thus, for our study, we chose Ni-Mn-Zn ferrites due to their promising properties and selected Cr^{3+} as a substitute to study the impact of Cr substitution on the properties of Ni-Mn-Zn ferrites.

The Cr^{3+}-substituted ($Co_{0.7}Cu_{0.3}Fe_{2-x}Cr_xO_4$) and Cu-Co ($Cu_{0.7}Co_{0.3}Fe_{2-x}Cr_xO_4$) nanoferrites were synthesized using the SGAC method by D. Parajuli et al. [57]. They looked at the morphological and structural characteristics. The replacement of Cr^{3+} ions causes them to decline gradually. The lattice parameter drops from 8.4441 Å to 8.4099 Å for Cu-Co nanoferrites and from 8.4498 Å to 8.4321 Å for Co-Cu nanoferrites. The reason for this decline is that Fe^{3+} ions have a higher ionic radius (0.645) than Cr^{3+} ions (0.615).

B. Venkata Suresh et al. [58] used the sol-gel method to produce the Cr^{3+} doped Co-Cu-Zn nano ferrites. They studied their magnetic and structural characteristics. The calculated lattice parameters in the present research case are marginally higher than the reported values [59], with an almost identical agreement. It is found that as the dopant concentration rises, the lattice parameter falls. The smaller ionic radius of Cr^{3+} (0.615 Å) cations may have replaced the greater ionic radius of Fe^{3+} (0.645 Å) cations, which might explain this [60, 61].

A.Y. Sleem et al. [62] studied the structural and magnetic properties of $Li_{0.4}Zn_{0.2}Cr_xFe_{2.4-x}O_4$ (x = 0.0, 0.1, 0.2, 0.3, 0.4, and 0.5) ferrites synthesized via citrate auto-combustion. The lattice parameter is shown to decrease as the chromium content rises. Cr^{3+} has a smaller ion radius (0.615 Å) than Fe^{3+} (0.645 Å), explaining this difference. As a consequence, replacing Cr^{3+} ions with Fe^{3+} ions decreases the lattice parameter. The structural and magnetic properties of lithium zinc ferrite were considerably changed when Cr was substituted with Fe. The magnetization decreased considerably as the Cr concentration rose. Neel's two-sublattice technique was utilized to study this phenomenon.

Chebbi et al. [63] used the SGAC process to produce Cr-substituted Mg-Co ferrite samples and studied their structural, optical, electrical, and dielectric properties. The study demonstrates a decrease in the measured lattice parameter as Cr replacement increases. They also found that substituting Cr for Fe reduced the average crystallite size.

References

[1] A. K. Singh, T.C. Goel, and R.G. Mendiratta. Journal of Applied Physics 91 (2002), 10.

[2] V.D More, S.R Kadam, S.B Shelke, P. Gaikwad, R.H .Kadam, S..T Alone. Biointerface Research in Applied Chemistry. 12 (2022), 4, 5021 – 5030.

[3] M. Kamran, M. Anis-ur-Rehman. Journal of Alloys and Compounds, 822 (2020), 153583.

[4] V.G. Deonikar, V.D. Kulkarni, S.M. Rathod, H. Kim. Inorganic Chemistry Communications. 119 (2020), 108074.

[5] J.C. Maxwell, Electricity and Magnetism. Vol. 1(1954), Section 328, Oxford University. Press, Oxford.

[6] W.A. Yager. Journal of Applied Physics. 7 (1936), 434- 450.

[7] C.G. Koops, Physical Review. 83 (1951), 121-124.

[8] A.S. Priya, D. Geetha, N. Kavitha. Materials Research Express. 5 (2018), 6.

[9] M. S. Hossain, M. B. Alam, M. Shahjahan, M. H. A. Begum, M. Hossain, S. Islam, N. Khatun, M. S. Alam, and M. A. Mamun, Journal of Advanced Dieletrics. 08 (2018), 1850030.

[10] C. G. Koops, Physical Review. 83 (1951) 121.

[11] K. W. Wagner, Annals of Physics. 40 (1973), 817.

[12] Y. Zhong, L. Zhongwen, C. Shengming, S. Yuerning, and S. Ke, Rare Metals. 25 Special Issue. 25 (2006) 584.

[13] H. A. Begum, N. Khatun, S. Islam, N. Ara Ahmed, M. S. Hossain, M. A. Gafur, and A. Siddika, International Journal of Nano Electronics and Materials. 11 (2018),1, [15-24]

[14] D. Ravinder, K. Vijay Kumar, Bulletin of Materials Science. 24 (2001) 505-509.

[15] M. Shahjahan, N. A. Ahmed, S. N. Rhaman, S. Islam, N. Khatun, M. S. Hossain, International Journal of Innovative Technology and Exploring Engineering (IJITEE). 3 (2014), 8.

[16] K. Iwauchi, Japanese Journal of Applied Physics. 10 (1971), 1520-1528.

[17] N. Rezlescu, E. Rezlescu, Physica Status Solidi (A). 23 (1974), 575-582.

[18] R. Das, S. Sarkar, Current Science. 109 (2015), 4, 25.

[19] M.M. Eltabey, W.R. Agami, H.T. Mohsen, Journal of Advanced Research**.** 5, (2014) 601-605.

[20] S. Chikazumi , S.H. Charap. Physics of Magnetism. New York, London, Sydney: John Wiley and Sons, Inc.; 1964

[21] S. Ramesh, B. Dhanalakshmi, B. Chandra Sekhar, P. S. V. Subba Rao, B. Parvatheeswara Rao, Applied Physics. A 122 (2016), 984.

[22] D. R. Mane, D. D. Birajdar, S. E. Shirsath, R. A. Telugu, R. H. Kadam. Physica Status Solidi A. 207 (2010), 10, 2355–2363.

[23] U.B. Gawas, V.M.S. Verenkar, V.T. Vader, Anil Jain, S. S. Meena, Materials Chemistry and Physics. 275 (2022) 125250.

[24] F. A. Ahmed · L. N. Singh, Journal of Materials Science & Surface Engineering. 6 (2018) 4, 825-830.

[25] V. K. Babbar and R. K. Puri, IEEE Transactions On Magnetics. 28 (1992) No. I.

[26] A.A. Sattar, H.M. El-Sayed, K.M. El-Shokrofy and M.M. El-Tabey, Journal of Applied Sciences. 5 (2005), 1,162-168.

[27]S. Ramesh, B. Dhanalakshmi, B.C. Sekhar, P.S.V.Subba Rao, B.P. Rao, Ceramics International. 42 (2016), 9591-9598.

[28] Jiajia Pei, Zhi Wang, Yu Gao, Haoming Zhang, Current Applied Physics. 19 (2019), 440-446.

[29] Vikram More, Supriya Kadam, Satish Shelke, Pravin Gaikwad, Ramkrishna Kadam, Suresh Alone, Biointerface Research in Applied Chemistry, 12, (2022), 5021 – 5030.

[30] S. Ramesh, L.N. Patro, B. Dhanalakshmi, B. Chandrasekhar, T. Anil Babu, K. Chandra Babu Naidu, B. Parvatheeswara Rao, Materials Chemistry and Physics, 306 (2023), 128055.

[31] Shankar Rao Lohar. Acta Chimica Slovensica, 64 (2017), 931-937.

[32] M. Hashim, S. Kumar, S.E. Shirsath, R.K Kotnala, H. Chung, R. Kumar, Powder Technology. 229 (2012), 37-44.

[33] Hashim, Alimuddin, M. Wasi Khan, S. Kumar, S.E. Shirsath, and R. Kumar, Advanced Nanomaterials and Nanotechnology. 143 (2013), 215-224.

[34] Y.M. Yakovlev, E.V. Rubalikaya, and N. Lapovok, Soviet Physics –Solid State. 10 (1969), 230.

[35] F. Alam, M.L. Rahman, M.H.R. Khan, A.K.M.A. Hossain, Journal of Modern Physics. 5 (2014), 1223-1233.

[36] A. K. Pradhan, P. R. Mandal, K. Bera, S. Saha, T. K. Nath, Physica B: Physics of Condensed Matter. 525 (2017), 1-6.

[37] C. Guilland and H. Creveaux. Comptes Rendus del'Academie des Science. 230(1950), 1256 (France).

[38] Pankaj Choudhary, Tarun Tyagi, M.A.Dar, and Dinesh Varshney. D.A.E. Solid State Physics Symposium. 2015.

[39] S. Mahalakshmi, K.S. Manja, Journal of Alloys and Compounds. 457 (2008), 552.

[40] K. Praveena, K. Sadhana, S. Matteppanavar, Hsiang-Lin Liu. Journal of Magnetism and Magnetic Materials. 423 (2017), 343-352.

[41] F. Alam, B. C Das, and A. K. M. Akther Hossain, Proceeding of 14th Global Engineering and Technology Conference. ISBN: 978-1-925488-60-9.

[42] R.M. Sebastian, S. Xavier, E. M. Mohammed, IJESIT, 2 (2013), 4.

[43] M. Raghasudha, D. Ravinder, and P. Veersomaiah, Journal of Chemistry. 4 (2013), 7.

[44] B.R. Karche, B.V. Khasbardar, A. S. Vaingankar, Journal of Magnetism and Magnetic Materials. 168 (1997) 3, 292.

[45] S.A. Masti, A. K. Sharma and P. N. Vasambekar. Advance in Applied Science Research. 4 (2013), 4, 335-339.

[46] A. Baykal, A. Z. Elmal, M. Sertkol, H. Sozeri, Journal of Superconductivity and Novel Magnetism . 28 (2015)11, 3405-3410.

[47] E. K. Senbeto, S. Elangovan, Journal of Nanomaterials, 2023(2023), Article ID 5103278, 9.

[48] Y. Koseoglu, M. I. O. Oleiwi, R. Yilgin, and A. N. Koçbay, Ceramics International. 38 (2012) 8, 6671–6676.

[49] S. Qamar, S. Yasin, N. Ramzan, T. Iqbal, and M. N. Akhtar, Materials Research Express. 6(2019), 11, Article ID 116104.

[50] S. E. Shirsath, B. G. Toksha, R. H. Kadam, S.M. Patage, D. R. Mane, G. S. Jangam and A. Ghashemi. Journal of Physics and Chemistry of Solids. 71(2010), 1669–1675.

[51] Kai Huang, Xiansong Liu, Shuangjiu Feng, Jiangying Yu, Xiaofei Niu, Faruilv, and Xing. From the journal High-Temperature Materials and Processes. 35(2016), 531-534.

[52] F.F. Lange and B.J. Kellet, Journal of the American Ceramic Society. 72(1989), 735–741.

[53] M. Azim, M. A. Chaudhry, N. Amin, M. I. Arshad, M. U. Islam, S. Nosheen, M. Ahmad, H. Anwar, M. Waseem, G. Mustafa, Digest Journal of Nanomaterials and Biostructures. 11 (2016), 953 – 962.

[54] M. N. Ashiqa, M. F. Ehsan, M. J. Iqbal, I. H. Gul, Journal of Alloys and Compounds. 509 (2011), 5119.

[55] S. Haque, S. C. Mazumdar, M. N. I. Khan, M. K. Das. Materials Sciences and Applications. 12(2021), 121-138.

[56] M. Saleem, D. Varshney, AIP Conference. Proceedings. 1953 (2018), 1.

[57] D. Parajuli, N. Murali, K. Samatha. BIBECHANA, 20 (2023), 275-284.

[58] Bade Venkata Suresh, G.V.R. Seshagiri Rao, E. Nirmala Devi, Govind Nandipati, Inorganic Chemistry Communications,165 (2024) 112534.

[59] T.W. Mammo, N. Murali, Y.M. Sileshi, T. Arunamani, Phys. B Condens. Matter, 531 (2018) 164–170.

[60] K. Chandramouli, V. Raghavendra, P.V.S.K. Phanidhar Varma, B. Suryanarayana, T.W. Mammo, D. Parajuli, P. Taddesse, N. Murali, Appl. Phys. A 127 (2021) 596.

[61] M.A. Munir, M.Y. Naz, S. Shukrullah, M.T. Ansar, M.U. Farooq, M. Irfan, S.N. F. Mursal, S. Legutko, J. Petru, M. Pag´ ac, Materials,15 (2022) 6890.

[62] A.Y. Sleem, N.I. Abu-Elsaad, S.A. Mazen, Bulletin of Faculty of Science, Zagazig University (BFSZU), 2023, 1, 24- 31

[63] M. Chebbi, S. Mansouri · S. Hcini, C. Bouzidi , N. Hamdaoui , L. El Mir, Journal of Electronic Materials. 54 (2025), 1475–1488.

Chapter 3: Materials and Methods

3.1 Introduction

Among the current issues encountered by researchers studying materials is synthesizing materials with the appropriate homogeneous composition, structural characteristics, and varied attributes suitable for specific uses. Materials synthesis for logic requires a comprehensive understanding of various factors crucial for achieving the desired materials, including the science of crystals, phase dynamics, and reactivity rates. Selecting a synthesis technique is crucial in establishing the physical characteristics of the materials. Various solid-state reactions, such as SGAC, chemical co-precipitation, hydrothermal, and micro-emulsion, can be employed to synthesize ferrite materials [1–5]. Therefore, carefully choosing the synthesis technique is crucial in regulating the composition, structure, morphology, and various properties of the investigated material. We have selected the SSR technique in the present case due to its low cost and easy synthesis process with desirable properties.

3.2 Solid-state reaction method

The SSR synthesis technique is one of the most commonly applied synthesis methods for producing large-scale products. The raw ingredients are mixed using either a wet or dry method. The ingredients are combined in a liquid instigator mill, an oscillating drum, or through dispersion in a moist blending process. This technique is highly efficient but requires additional energy to dewater and dry the material. Ball mills and drum mills are commonly used for dry mixing.

The approach relies on the interdiffusion of the components in a solid state. Generally, at ambient temperatures, materials do not react on the time scales typically seen. High temperatures are required so that the diffusion length (2Dt) 1/2, where t is the shooting time and D is the spreading constant for the species that diffuses quickly, is larger than the particle size. Next, in oxygen or air, the powders are calcined at temperatures greater than 1000°C. This procedure is repeated until the desired crystalline phase is achieved in the mixture. After being calcined, the powders are crushed again to a fine consistency. The calcined powders are formed into pellets or toroidal samples employing atmospheric or isostatic pressure or die-punch assembly. There are different atmospheres (air, oxygen, and nitrogen) during sintering, which is done in solid form at temperatures between 1000 - 1500°C for 1-4 hours at a time [6-8].

The solid-state process that leads to the creation of ferrite MFe_2O_4 can be expressed as follows:

$MO + Fe_2O_3 \rightarrow MFe_2O_4$; where the divalent ion is denoted by M.

3.3 Sample preparation

The synthesis was done using the solid-state reaction technique $Ni_{0.6}Mn_{0.2}Zn_{0.2}Cr_xFe_{2-x}O_4$ ferrites (where x=0.00, 0.05, 0.10, 0.15, 0.20). The basic ingredients utilized were powders with very high purity levels; these included NiO (99.9%), MnO (99.9%), ZnO (99.9%), Cr_2O_3 (99.9%), ZnO (99.9%), and Fe_2O_3 (99.9%), all of which are commercially accessible.

The required raw materials were measured precisely and then combined using a ceramic mortar and pestle for manual grinding. They added a few drops of acetone during the hand-milling process to further enhance the mixing quality. The compositions were calcinated at 800°C for 4 hours. Upon impact, the calcined powder was once again reduced to a fine powder. After adding 1 g weight percent polyvinyl alcohol (PVA) as a binder, samples in the form of pellets, discs, or toroid shapes were prepared by uni-axial pressing at 10 kN/cm^3 and 15 kN/cm^3, respectively. At 1100°C, the compact was sintered in a muffle furnace. The samples were heated and refrigerated at a rate of 5°C/min during the sintering procedure. Samples with varying surface morphology, electric and magnetic characteristics, and sintering temperatures were anticipated. The details of each step are explained below.

3.3.1 The raw materials

The solid-state reaction approach was used to manufacture samples of Ni-Mn-Zn ferrites with Cr^{3+} substitution. The fundamental composition of the ferrites was $Ni_{0.6}Mn_{0.2}Zn_{0.2}Cr_xFe_{2-x}O_4$ ($0.00 \leq x \leq 0.20$; in a step of 0.02). The raw materials utilized in this study consisted of Nickel oxide (NiO), Manganese oxide (MnO), Zinc oxide (ZnO), Iron oxide (Fe2O3), and Chromium oxide (Cr2O3), all of which were purchased from E. Merck Germany and possessed a purity level of 99.98%.

3.3.2 Weighted by stoichiometric ratio

Table 3.1: Weighted percentage for 15gm of $Ni_{0.6}Mn_{0.2}Zn_{0.2}Cr_xFe_{2-x}O_4$ with varying X is listed in Table.

x	NiO (gm)	MnO_2 (gm)	ZnO (gm)	Cr_2O_3 (gm)	Fe_2O_3 (gm)
0.0	2.8230	1.0950	1.0250	0	10.0569
0.05	2.8254	1.0959	1.0258	0.2395	9.8132
0.10	2.8277	1.0968	1.0267	0.4793	9.5693
0.15	2.8300	1.0977	1.0275	0.7196	9.3250
0.20	2.8323	1.0986	1.0283	0.9603	9.0803

3.3.3 Mixing by milling

The initial elements were weighed in the correct equilibrium ratios. Subsequently, employing a piece of pottery grinder and crushing, the ingredients were milled by hand for 6 hours to mix the oxide powders homogeneously.

3.3.4 Pre-sintering

There was only manual force used to compact the powder in a hydraulic press before it was put in a glazed crucible, and pre-sintering was done there for four hours at a constant 800°C. At the Material Science section, AECD, the materials were pre-sintered in a furnace called Nabertherm. The rate of cooling and heating was 5°C/min. Because ferrite generates its component oxides during this sample preparation stage, pre-sintering is quite essential. Counter diffusion is actually how the solid-state events that result in the creation of ferrites are carried out. This indicates that more than one kind of ion, initially moving in opposing directions between the two interacting interfaces of various oxide components, is involved in the diffusion. During the pre-sintering phase, spinel ferrite is created by the following reactions between Fe_2O_3 and metal oxides of MO or M_2O_3 (where M represents the atom of the divalent metal and here represents the atom of the trivalent metal) in the solid state:

$$MO + Fe_2O_3 \rightarrow MFe_2O_4 \text{ (spinel)}$$

$$2M_2O_3 + 4Fe_2O_4 \rightarrow 4MFe_2O_4 + O_2$$

3.3.5 Milling

By grinding the ferrite down to a size of 1 micron, intra-particle pores are removed, and the material is mixed until it is homogeneous. Grinding the powder and analyzing its characteristics, including particle size, morphology, consistency, extracted molecules, contaminants, and the intra-particle number of holes, are essential steps toward a successful sintering process. There needs to be careful monitoring to reduce iron contamination caused by the consistent wear of the mill wall and steel balls.

3.3.6 Shaping by pressing

Polyvinyl alcohol, in the form of a homogenous powder, has now been applied to the soil. The powder can be compacted using either the traditional approach, involving an assembly with a die and punch, or the more modern method of compression by water or isocratic force to achieve the required shape. We put the former to use. This method is challenging to press a uniformly dense mass due to the powder's friction gradient at the die walls and between particles. Adding lubricants, such as stearic acid, to the powder helps somewhat alleviate this issue. We mainly produced tablet and toroid forms of our samples. The specimen was compressed in a hydraulic press at 10kN/cm^3 for tablets and 15kN/cm^3 for toroids.

3.3.7 Final Sintering

Final sintering occurred in a porcelain crucible at 1100°C for 4 hours, where the tablets and toroids were placed. In powder sintering, the green compact, or crushed powder portion, is heated to a specific temperature and held there for a predetermined time. Sintering temperatures are typically 70–90% of the powder metal's melting point. As a result, the powder particles in the compact will form bonds with one another. The green compact bonds poorly; thus, this pressed, unsintered piece has only enough strength to be handled. Sintering bonds the material together, significantly increasing the strength of the component.

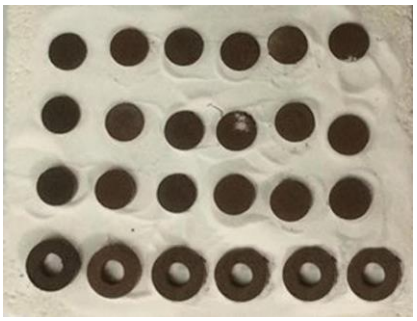

The flow chart below illustrates the primary phase in this procedure:

Fig. 3.2: Ring and Disc samples prepared by Hydraulic press.

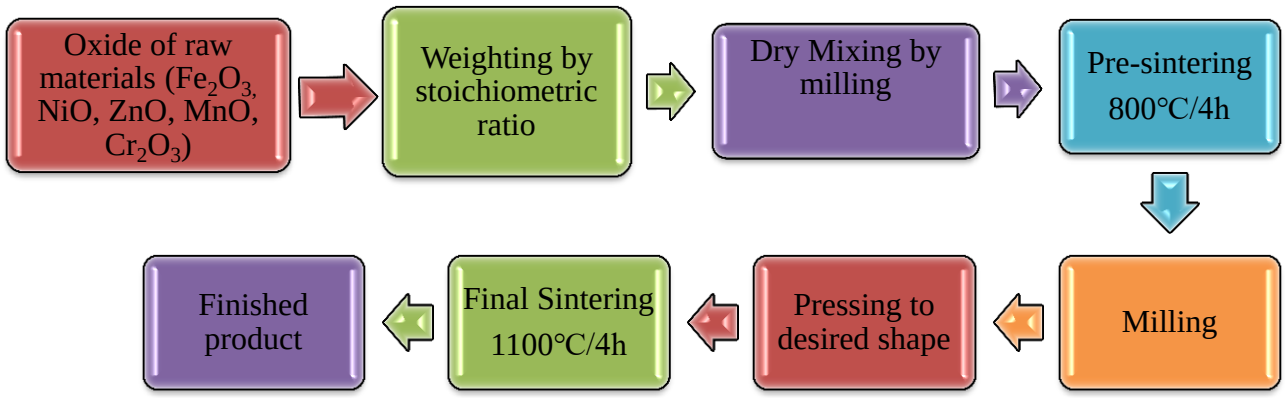

3.4: Experimental Techniques

3.4.1 Structural and Physical Properties Measurement

The determination of concentration, density, phase recognition, equilibrium dimension, structure of the crystal, measurement of grains, etc., are all part of this research. The XRD, SEM, and different measurement techniques outlined below were used to characterize the prepared samples studied herein.

3.4.1.1 X-ray diffraction technique

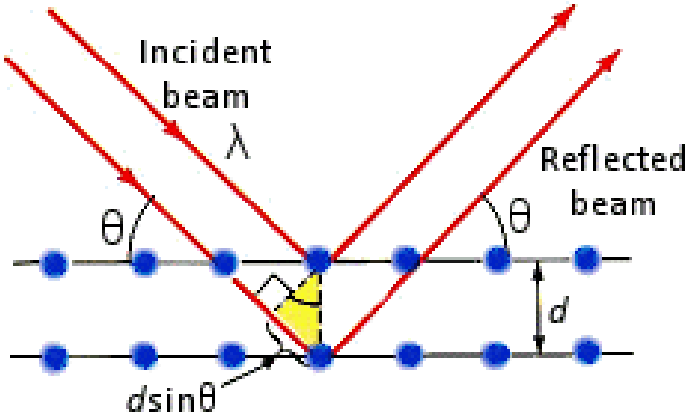

An efficient and non-destructive approach is the X-ray diffraction technique for determining a material's crystal structure. The interatomic gap corresponds to the peaks that are seen in an X-ray diffraction pattern. In this analysis, we shall examine the relationship between an incident X-ray beam and a periodic arrangement of atoms, as depicted in the two-dimensional picture. The depicted spheres in the figure can be interpreted as atoms, which are organized into distinct planes inside the crystal structure. The necessary condition for divergence (peak) to happen for a specific set of planes of a lattice with an inter-plane distance of d is denoted by the simple formula

$$2d \sin\theta = n\lambda$$

The phenomenon referred to as Bragg's law is widely recognized in the field. The X-ray wavelength is represented by the symbol λ in the preceding equation, the scattering angle by θ, and the order of the diffraction peak by the number n. When interpreting X-ray diffraction data, Bragg's Law is crucial. According to legal principles, it is established that diffraction can occur only under the condition that the wavelength (λ) is less than twice the distance (2d) [10].

Fig. 3.3 : Bragg's diffrection pattern

The structural phase identification of the synthesized sample was done in the MSD at the AECD, using a PHILIPS PW 3040 X‟pert PRO X-ray diffractometer.

3.4.1.2 Lattice Constants and Identification of Phase

The samples' structural properties, including the lattice parameter and component phase, were determined using the XRD data, which contains the θ_{hkl} and d_{hkl} values associated with different crystallographic planes. Bragg's diffraction equation is often used to calculate the lattice constants of the ferrites. The lattice spacing (inter-planar distance), d, is found by utilizing reflections, and the equation that follows is used for this determination.

$$2d_{hkl}\sin\theta = \lambda$$

$$\text{i.e., } d_{hkl} = \frac{\lambda}{2\sin\theta}$$

When the diffraction placement is shown by θ, the spectral length of the X-ray is conveyed by λ, and the diffraction compliance is indicated by an integer, n.

For every peak in every sample, the lattice constant was determined using the following formula:

$$a = d_{hkl}\sqrt{h^2 + k^2 + l^2}$$

The factors h, k, and l show the dimensions of the crystal surfaces. The computer program "X Pert HJGHS CORE" gets the d_{hkl} values. For different reflection planes, denoted as a, a_1, a_2, a_3, and so forth, different *a* values were obtained. The accurate lattice constants for every sample were determined using the Nelson-Riley (N-R) extrapolation technique. The Nelson-Riley function is used to display the lattice parameter values of each reflected plane. The N-R function F (θ) has the following equation.

$$F(\theta) = \frac{1}{2}\left[\frac{\cos^2\theta}{\sin^2\theta} + \frac{\cos^2\theta}{\theta}\right]$$

where θ is Bragg's angle. Using the extrapolation approach, the value of the lattice parameter a_0 was calculated with an estimated error of ± 0.0001Å by plotting the graph of the lattice parameter *a* against the function F (θ).

3.4.1.3 X-ray Density and Bulk Density

The X-ray density was calculated using the following equation:

$$d_x = \frac{8M}{N_a a_0^3}$$

The equation provided relates the molecular weight M of a given composition to the lattice constant a and Avogadro's number N_a (6.023×10^{23} $mole^{-1}$).

The calculation of bulk density involved the consideration of a cylindrical pellet with a given mass (m) and volume (V) of the pellets, utilizing the appropriate mathematical relationship

$$d_B = \frac{m}{V} = \frac{m}{\pi r^2 h}$$

The particle sample's mass, radius, and thickness are represented by the variables "m," "r," and "h" in the context provided.

3.4.1.4 Porosity

The sintering process of oxide materials results in the development of porosity, which is an inherent property. The impact of porosity on the physical and electromagnetic attributes of the examined specimens is of significant importance. The X-ray density (d_x) and bulk density (d_B) were compared to determine the measurement. The following formula has been used to determine the porosity percentage [11].

$$P = \left(1 - \frac{d_B}{d_x}\right) \times 100\%$$

3.4.2 Scanning Electron Microscope (SEM)

BUET, Dhaka, provided a SEM for observing the microstructure of the samples.

3.4.3 Energy Dispersive Spectrometer (EDS)

In conjunction with SEM, a chemical microanalysis technique known as energy-dispersive X-ray spectroscopy (EDS or EDX) is employed. The elemental composition of a given volume was characterized using the EDS method, which involves identifying *X*-rays liberated from the material when irradiated by an electron beam. The smallest measurable features or phases are typically under 1μm in size.

3.5 Electrical Properties Measurement

The impedance analyzer (Model: Wayne Kerr 6500B) was employed to ascertain the electrical properties, which included electrical conductivity, resistivity, and dielectric constant.

3.5.1 Dielectric Relaxation

The frequency dependence of dielectric constant measurements was taken from 1 kHz to 100 MHz using a Hewlett-Packard (model no. 4192A) Impedance Analyzer. Each pellet's two surfaces were covered using silver paste as a conductive medium for electrical and dielectric evaluations, and they were carefully refined to eliminate any abrasiveness. The actual value of the dielectric constant was computed by the formula;

$$\varepsilon' = CL/\varepsilon_0 A$$

Where C signifies capacitance, L denotes thickness or height, A is the surface area of the pellet, and ε_0 stands for the constant permittivity of empty space.

The dielectric constant's imaginary component was determined by employing the following formula;

$$\varepsilon'' = \varepsilon' tan\delta$$

The loss factor, or imaginary component, equals zero for perfectly lossless materials. It is the rate at which energy leaves a material when subjected to an applied electric field. Loss tangent:

$$tan\delta = \frac{\varepsilon''}{\varepsilon'}$$

3.5.2 Electric Modulus

The energy or configuration distribution of ions within a specific structure is quantitatively represented by the spectrum of the complicated electric modulus. Moreover, it elucidates the microscopic properties and electrical relaxation of ferrites. The formalism of modulus has been implemented to mitigate the impact of polarization effects occurring at the interface of the electrodes. Therefore, the spectra of the complex modulus M of electricity indicate the sample's exclusive dynamic features. The calculations for the electric modulus and its real and imaginary components were derived from the utilization of the following equations:

$$M^* = {}^1/_{\varepsilon^*}$$

$$M' = \frac{\varepsilon'}{(\varepsilon'^2 + \varepsilon''^2)}$$

$$M'' = \frac{\varepsilon''}{(\varepsilon'^2 + \varepsilon''^2)}$$

Where M*, M', and M'' represent the elaborate electrical modulation, the actual and fictional regions of the electrical modulation, correspondingly.

3.4.1 Impedance Spectroscopy

Modulus plots in the complex plane provide supplementary information conveyed by impedance plots in the complex plane. Employing the established relationships, the real component of impedance data is computed, as documented in the reference [12].

$$Z' = \frac{M''}{\omega C_0}$$

And the imaginary part,

$$Z'' = \frac{M'}{\omega C_0}$$

3.5.3 Magnetic properties measurement

Ferrites exhibit magnetization due to a discrepancy in magnetic moments between their two sub-lattices. The magnitude of the resultant magnetization increases as the variation in the moments inside the two sub-lattices becomes higher, owing to the anti-parallel arrangements of these moments. A net magnetic moment's existence, which leads to magnetization, is a consequence of the disparities between the two sub-lattices in the magnetic moment. The current investigation involved the utilization of a VSM to carry out magnetization. A VSM was employed to measure the magnetic properties at the Materials Science Division of the AECC in Dhaka.

3.6 Permeability Measurement

The impact of thermal treatment at various temperatures on the evolution of permeability and magnetic loss components in a ferrite sample was investigated by analyzing the frequency dependence of complex permeability. A toroid-shaped sample, fabricated using insulating copper wire, was utilized for this purpose. As shown in Figure 4.5, the WK 6500B Impedance analyzer is capable of directly measuring the loss factor and the inductance value, represented by L.

$$D = tan\delta$$

The actual part of the complex permeability, μ', can be determined by utilizing the relationship derived from inductance,$\mu' = \frac{L}{L_0}$

The inductance of the toroid, denoted as L, can be compared to the inductance of a coil with the same geometric shape in a vacuum, denoted as L_0.

The determination of Lo is achieved by utilizing a specific relation.

$$L_0 = \frac{\mu_0 N^2 S}{\pi \bar{d}}$$

In this context, μ_0 represents the permeability of the vacuum, N denotes the number of turns (specifically, N = 5), and S refers to the cross-sectional area of the toroid-shaped sample. It should be noted that S is calculated as the product of d and h, where d and h represent the respective dimensions of the sample.

$$d = \frac{d_1 \sim d_2}{2}$$

The toroid sample's average diameter is denoted by $\bar{d}$

$$\bar{d} = \frac{d_1 + d_2}{2}$$

Where d_1 and d_2 are the toroid samples' center and exterior diameters, respectively.

References

[1] A. Gruskeva, J. Slama, R. Dosoudil, M. Usakova, V. Jancarik, E. Usak. Journal of Magnetism and Magnetic Materials. 320 (2008), 860-864.

[2] A. A. Pandit, S. S. More, R. G. Dorik, K. M. Jadhav. Bulletin of Materials Science. 26 (2003), 17.

[3] M. George, A. M. John, S. S. Nair, P. A. Joy, M. R. Anantharaman, Journal of Magnetism and Magnetic Materials. 302 (2006), 190-195.

[4] J. Wang, Journal of Materials Science and Engineering. B 127 (2006) 81.

[5] N. Moumen, M. P. Pileni. Chemistry of Materials. 8 (1996), 1128-1134.

[6] B. D. Cullity, Introduction to Magnetic Materials, Addison-Wesley Publishing Company, Inc, California (1972)

[7] R. J. Brook, Sintering: An Overview, Concise Encyclopedia of Advanced Ceramic Materials, Pergamon Press, Oxford. (1991) 438.

[8] P. Reijnen, Science of Ceramics, Academic Press. London, (1967).

[9] K. O. Low, S. R. Frank, Journal of Magnetism and Magnetic Materials. 246 (2002), 30-35.

[10] T. Abbas, M. U. Islam, M.C. Ashraf, Modern Physics Letters B, 9 (19195), 419.

[11] J.Smit and H.P.J. Wijn —Ferrites, Philips Technical Library C Wiley, New York, 1959.

[12] S. Upadhyay, D. Kumar, O. Parkash. Bulletin of Materials Science. 19 (1996), 513.

Chapter 4: Results and Discussion

4.1 Structural Properties

4.1.1 X-Ray Diffraction Analysis

Cr-substituted Ni-Mn-Zn ferrites' XRD patterns (X-ray diffraction), which have the chemical makeup of $Ni_{0.6}Mn_{0.2}Zn_{0.2}Fe_{2-x}Cr_xO_4$ (x = 0.0, 0.05, 0.10, 0.15, and 0.20) (NMZCFO), are shown to have been heated at 1100 °C in Fig. 4.1. The successful synthesis of the targeted samples is true because the tops are visible, (111), (220), (311), (222), (400), (422), (511), and (440), noted for spinel structures. Moreover, it is confirmed that no secondary peak is found for all samples. The structural characteristics of the synthetic materials will also be examined using XRD.

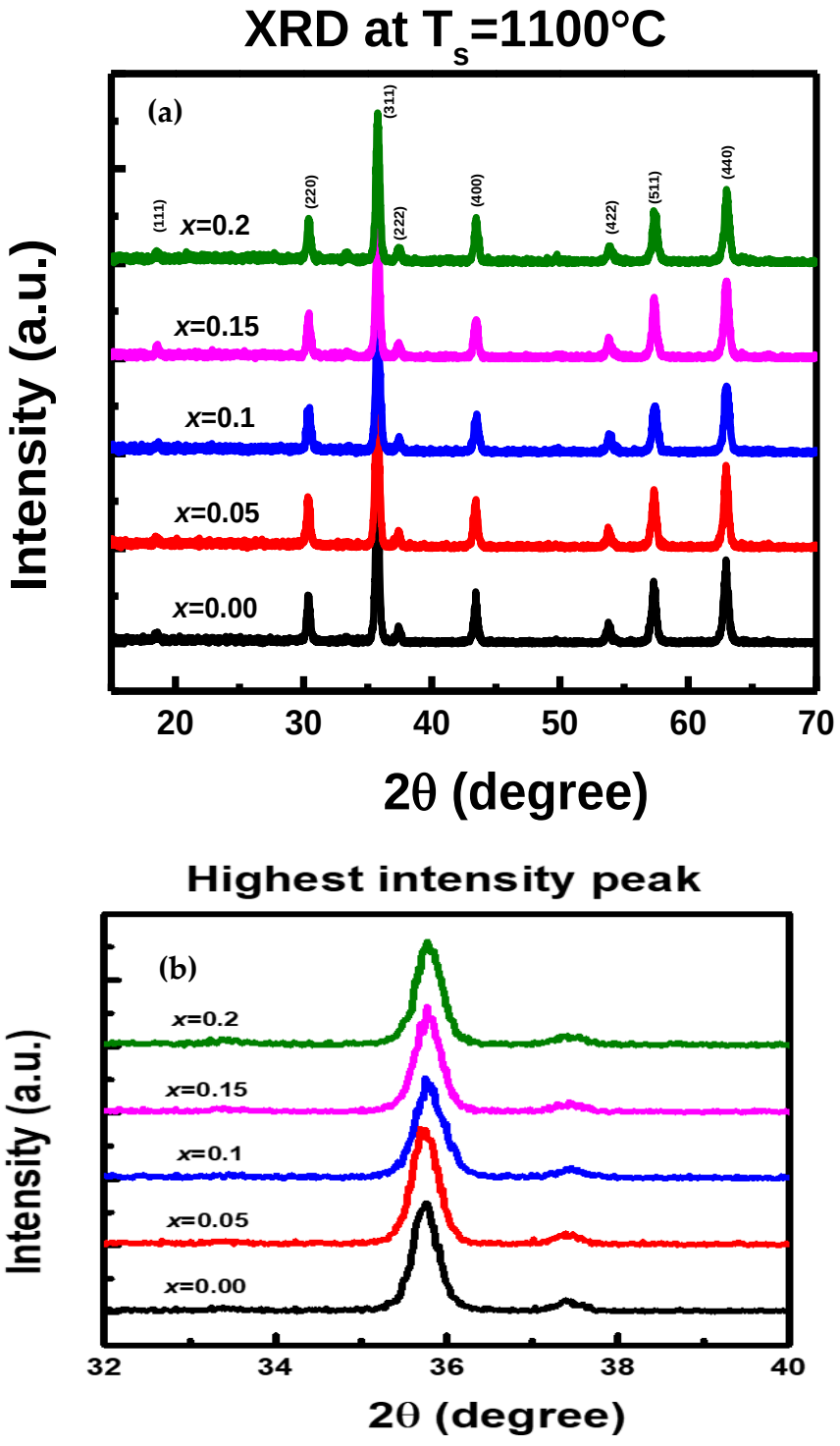

Fig. 4.1: (a) The XRD patterns of Cr^{3+} substituted $Ni_{0.6}Mn_{0.2}Zn_{0.2}Cr_xFe_{2-x}O_4$ ferrite samples; (b) highest peak intensity.

4.1.2 Lattice Constant

The formula $a = d\sqrt{h^2 + k^2 + l^2}$, where h, k, and l are the Miller indices of the planes as indicated by the peaks in the XRD data of the samples, has been employed to ascertain the lattice constant (a), in Fig. 4.2. The N-R extrapolation technique was employed to measure the lattice constants. F (θ) = 1/2 [(cos² θ)/sin θ +(cos² θ)/ θ], where θ is Bragg's angle, is the definition of the N-R function, F (θ) [1]. For each sample, the lattice value was found by extrapolating all peaks to F (θ) =0 or θ =90° [2]. The change of the lattice constant (a) decreases as the chromium concentration rises, except for x = 0.20 [3, 4]. In the ferrite composition, the Fe^{3+} ions (0.645 Å) are substituted by the comparatively smaller Cr^{3+} ions (0.63 Å), which causes a decrease in lattice constants [5]. Similar declination of the lattice constants due to Cr^{3+} ions substitution in other ferrites is also reported [6, 7]. The magnetic ions' jump length is computed by a in the A-site and B-site. Thus, a decrease in the ion jump length (L_A and L_B) is expected [8]. In addition, the value of a for parent composition is also consistent with the reported value [9].

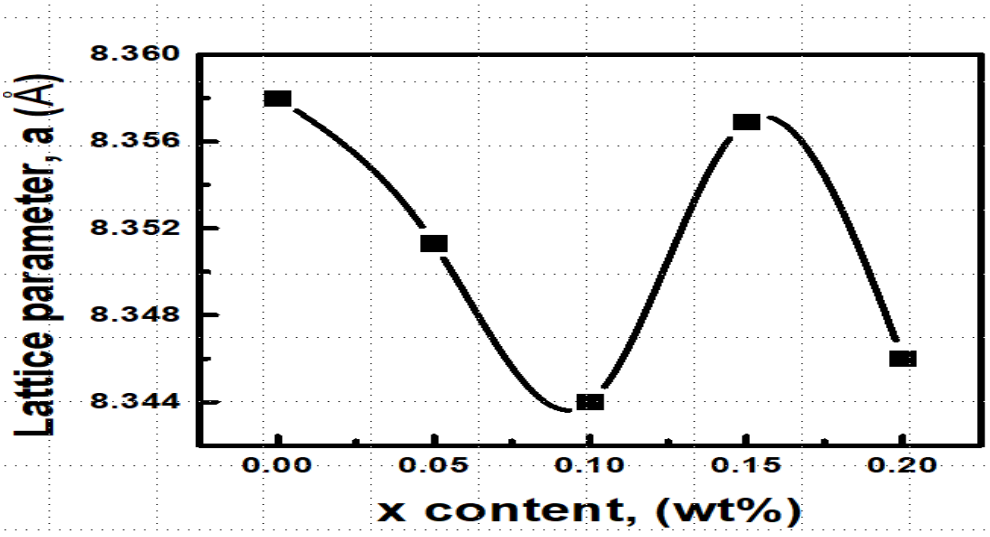

Fig.4.2: The fluctuation in lattice parameter with X content.

4.1.3 Density and Porosity

The bulk density was determined by applying the molecular weight and unit cell volume to the calculation of X-ray density for each sample, as opposed to relying on conventional mass and measurements. Fig.4.3. demonstrates how Cr^{3+} affects NMZCFO's bulk and x-ray densities. As seen, the bulk density decreases gradually with increasing Cr contents, and the atomic weights of Cr and Fe help to explain. The atomic mass and density of Fe are higher than those of Cr, causing a reduction in the density of the synthesized samples. Additionally, comparable outcomes have been documented by Subramani et al. [2, 10]. The density of X-rays is greater than that of the bulk. Usually, some pores have developed during the synthesis of materials, which have not been considered in X-density calculation; consequently, higher values are expected.

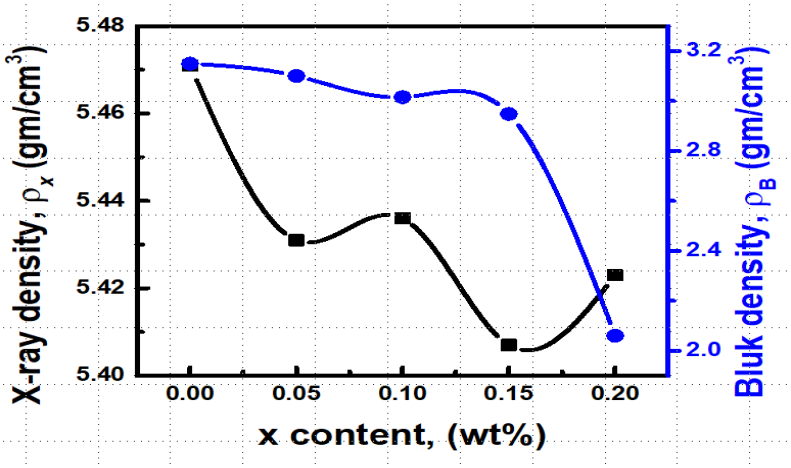

Fig. 4.3: The effect of Cr^{3+} substitution on the theoretical and physical density of the synthesized samples.

Table 4.1: Lattice Parameter, X-ray Density, Bulk Density, Porosity, and Average Grain Size of $Ni_{0.6}Mn_{0.2}Zn_{0.2}Cr_xFe_{2-x}O_4$.

x	a (Å)	ρ_x(gm/cm^3)	ρ_B(gm/cm^3)	P(%)	Dg (μm)
0.00	8.3579	5.471	3.149	42.44	0.556233
0.05	8.3513	5.431	3.1	42.92	0.469733
0.10	8.344	5.436	3.015	44.53	0.578333
0.15	8.3569	5.4072	2.948	45.48	0.554767
0.20	8.346	5.423	2.060	62.013	0.521767

4.2 Morphological study of $Ni_{0.6}Mn_{0.2}Zn_{0.2}Cr_xFe_{2-x}O_4$ (x=0.00, 0.05, 0.10, 0.15, 0.20)

The present work examines the surface morphology and microstructure of $Ni_{0.6}Mn_{0.2}Zn_{0.2}Cr_xFe_{2-x}O_4$ (x = 0.00, 0.05, 0.10, 0.15, 0.20) ferrites. The scanning electron microscope (SEM) is employed to analyze the ruptured surfaces, as depicted in Figure 4.4. According to the SEM pictures, the samples are tightly packed, free of cracks, and have a uniform grain distribution with distinct grain boundaries throughout. Since the ferrites have a uniform distribution, they use the pushing force of the grain boundary within each grain to get a uniform grain size distribution [11]. Grain size alteration significantly impacts ferrite's electric and magnetic characteristics. By including a sufficiently large number of grains were extracted from the materials' surface micrographs, and their sizes were calculated using the ImageJ program [12] and the linear intercept method. Fig.4.4. depicts how the samples' grain size varies depending on the Cr content. Except for when x = 0.10, the grain size initially decreases with increasing Cr^{3+} ions. The interaction between the force that impels the force that is exerted by the particle boundary movement, pores imposed on the grain development in the samples has a significant impact [11].

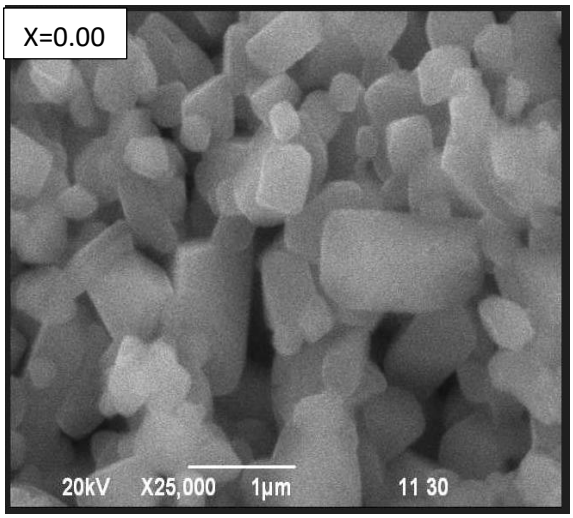
X=0.00
20kV X25,000 1µm 11 30

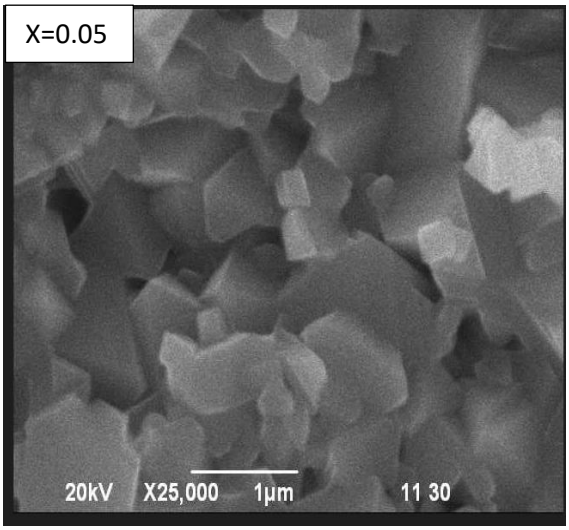
X=0.05
20kV X25,000 1µm 11 30

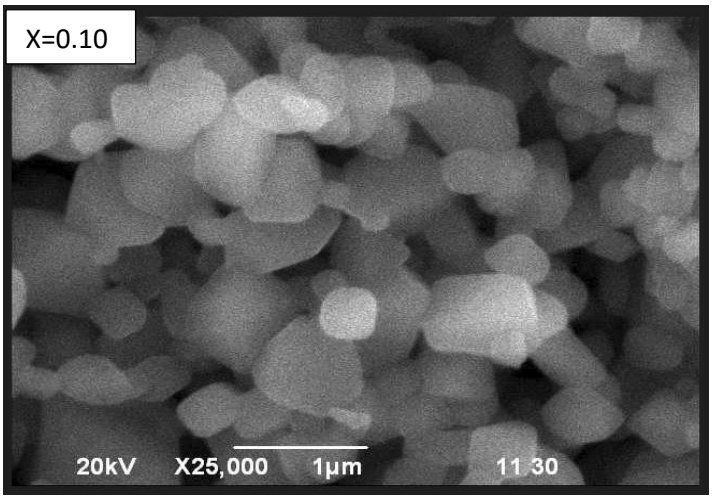
X=0.10
20kV X25,000 1µm 11 30

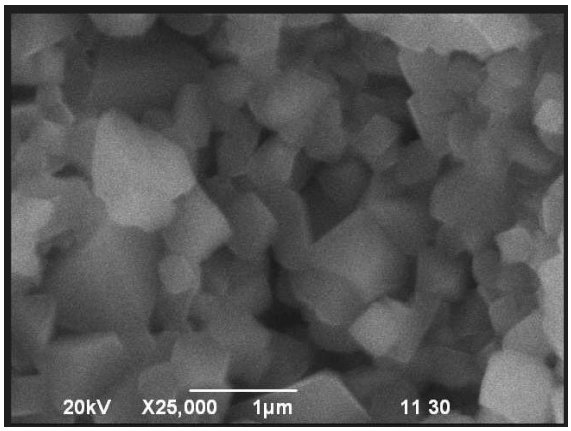
20kV X25,000 1µm 11 30

X=0.15

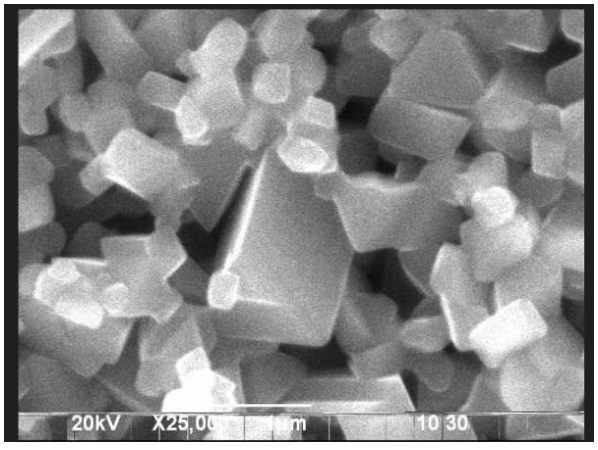
20kV X25,00 m 10 30

X=0.20

Fig. 4.4: SEM spectra of $Ni_{0.6}Mn_{0.2}Zn_{0.2}Cr_xFe_{2-x}O_4$ ferrites (x=0.0, 0.05, 0.10, 0.15, 0.20).

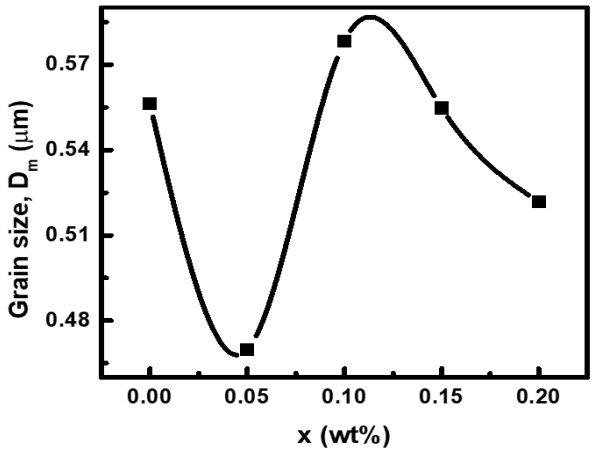

Fig. 4.5: The variation of grain size patterns of Cr^{3+} substituted $Ni_{0.6}Mn_{0.2}Zn_{0.2}Cr_xFe_{2-x}O_4$ ferrite samples (x=0.00, 0.05, 0.10, 0.15, 0.20).

4.3 Electrical Properties of $Ni_{0.6}Mn_{0.2}Zn_{0.2}Cr_xFe_{2-x}O_4$ Ferrite

4.3.1 Dielectric Relaxation Properties

The dielectric coefficient and loss tangent of the NMZCFO ferrites are determined by [$\varepsilon'=Cd/\varepsilon_0 A$], where C stands for capacitance, d for diameter, ˆ ε_0 for free-space conductivity, and A for pellet area, respectively, and are shown in Figure 4.6 (a) and (b). As is typical for spinel ferrites, the curves imply an enormous drop at a low frequency of up to 100 kHz, followed by a bit of a sluggish decline, and finally, a nearly negligible and frequency-independent decrease across excessive frequencies [13]. The behavior is comparable with previous results seen in several ferrite systems, including Mg-Zn [14], Sm, Cr, and Co substituted Mg-Zn ferrites [15, 16, 17], $Mg_{0.6}Co_{0.4}Fe_{2-x}Cr_xO_4$ [7], and Ni-Zn [18, 19].

Since the Maxwell-Wagner model is comprised of two layers of dielectric materials, Koops' theory can describe the behavior that is reliant upon the frequency of the NMZCFO [20, 21].

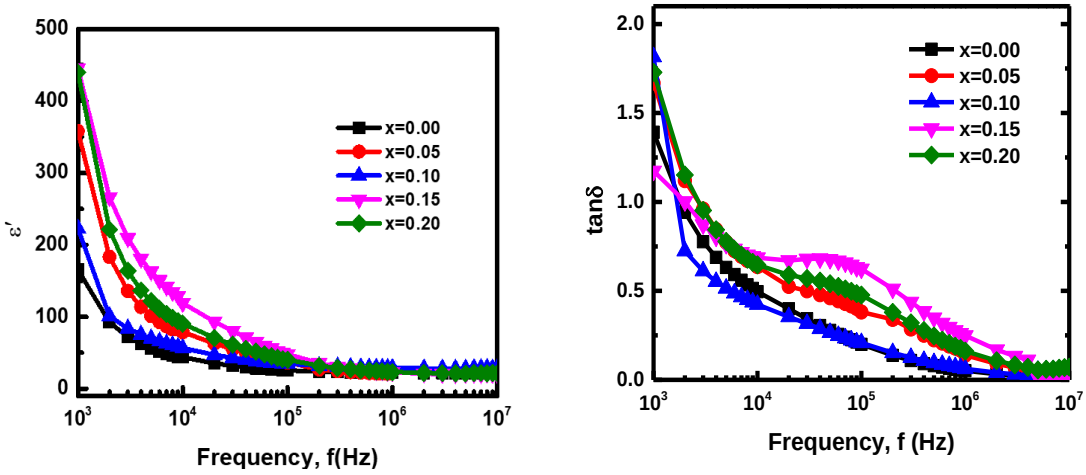

(a) **(b)**

Fig. 4.6: The frequency-dependent dielectric constant (a) and dielectric loss (b) of $Ni_{0.6}Mn_{0.2}Zn_{0.2}Cr_xFe_{2-x}O_4$; (x=0.00, 0.05, 0.10, 0.15, 0.20) ferrites at room temperature.

The samples with Cr^{3+} substituted had a higher dielectric efficiency than the original sample (x = 0). This alteration is related to the variation of the microstructure in addition to composition. The low-frequency spectrum's polarization is determined by the electron exchange between Fe^{2+} and Fe^{3+} and, therefore, the localized transfer of charges across areas in the direction of the applied field. The inability to detect the applied electric field at high frequencies results in a reduction and a fixed value in electron transport between Fe^{2+} and Fe^{3+} [22]. Figure 4.6 (a) displays the dielectric loss (tan δ) and frequency-dependent dielectric constant (ε′) of distinct $Ni_{0.6}Mn_{0.2}Zn_{0.2}Cr_xFe_{2-x}O_4$ ferrites at varying concentrations of Cr. Similar to other spinel ferrites, the samples exhibit typical frequency-dependent behavior. In particular, the dielectric constant

widens in low-frequency regions and decreases in wider frequency ranges in a frequency-dependent manner. The phenomenon is succinctly explained by the Maxwell–Wagner two-layer model, which varies with frequency, by considering the polarization of space charges [23]. Polycrystalline materials typically comprise conductive grains enclosed by insulating grain borders. At low frequencies, a significant increase in changes in the dielectric constant is caused by the formation of interfacial polarization. This polarization arises from the alignment of charge carriers at the interfaces between grains in response to an external field [24]. However, as the frequency increases, charge conductors are unable to align themselves quickly enough with the changing frequency, resulting in decreased values of ε' [25].

The energy loss that occurs during the polarization process is reflected by the dielectric tangent loss (tan δ), a major parameter. It is observed that as the frequency increases, the tangent loss typically decreases. A distinct peak in tangent loss occurs in the sample with a composition of x=0.05, 0.15, and 0.20 at around 800 kHz. A correlation can be established between the electron shifting frequency regarding Fe^{2+} and Fe^{3+} and this peak, which follows the frequency of the electric field that is being applied [26]. As observed in Figure 4.6(b), the curves for substituted compositions show a standard highest value, including a peak at a certain frequency. Based on the graphs, it appears that there is a maximal frequency [$\omega = 2\pi f_{max}$ and τ is the relaxing time, which is correlated with the leaping probability per unit time p using the expression $\tau = 1/2p$]. The intensity of the applied electric field is approximately equivalent to the frequency of jumps between Fe^{2+} and Fe^{3+} ions at proximate B-sites [27].

4.3.2 Electric Modulus Analysis

The materials' electrical response is neither homogeneous nor inhomogeneous, and the complex electric modulus has done a commendable job of studying the electrical

relaxation in materials that are electrically and ionically accompanied by a microscopic feature of the materials [28].

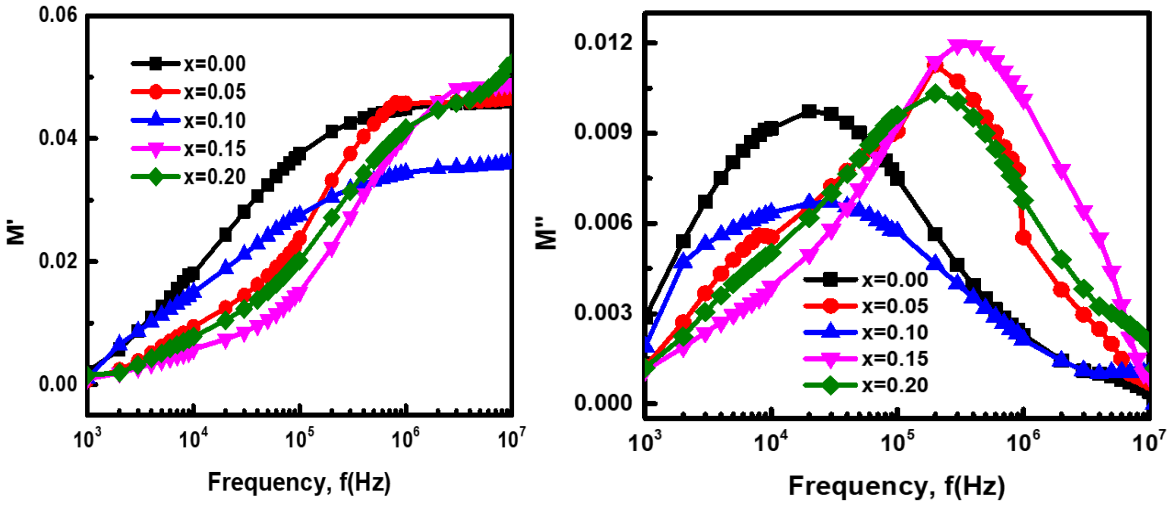

(a) **(b)**

Fig. 4.7: The real part of (M′) (a) and imaginary part (M″) (b) of electric modulus for $Ni_{0.6}Mn_{0.2}Zn_{0.2}Cr_xFe_{2-x}O_4$ as a function of frequency.

Figures 4.7(a) and (b) depict the actual and fictitious components of the modulus, as determined by the equation shown below:

$$M' = \frac{\varepsilon'}{\varepsilon'^2+\varepsilon''^2} \quad \text{and} \quad M'' = \frac{\varepsilon''}{\varepsilon'^2+\varepsilon''^2}$$

The frequency dependency of the samples' actual electric modulus (M) values is shown in Fig. 4.7(a). The value of M' exhibits that the contribution of electrode polarization is insignificant in the produced ferrites [29] by attaining a peak in the higher frequency side and null in the lower frequency side. With the complex electric modulus [$M^*= M' + jM''$, $M'=\varepsilon'/(\varepsilon'^2 + \varepsilon''^2)$ and $M''=\varepsilon''/(\varepsilon'^2 + \varepsilon''^2)$], the frequency-dependent imaginary component of the electric modulus M″ is shown in Fig. 4.7 (b). From the samples' M″ values, it is possible to determine the smallest capacitance and the highest resistance. Either long-range or

short-range charge carrier movement is the source of the relaxing process [30]. According to Sinclair and West's idea [14], the graphs demonstrate a wide range in the process, with different frequencies of the peaks. The curves deviate from Debye-like behavior, and the separation of the peaks indicates localized charge carriers being present.

4.3.3 Impedance Spectra and Cole-Cole Plot

In a Cole-Cole plot, it is typical to observe two successive semicircles. The first semi-circle represents the resistance at the grain boundaries, while the second semi-circle represents the grains resistance contribution. Figure 4.8 demonstrates that the complex impedance plot displays a single semicircle for each sample's composition.

The statement suggests the prevalence of resistance at the grain boundaries. The development of an insulating layer may be suspected as the cause of the observed particle boundary resistivity in the current samples. As the chromium content of ferrite increases, the grain and boundary resistivities rise and fall, respectively. This outcome is likewise achieved by other studies [31].

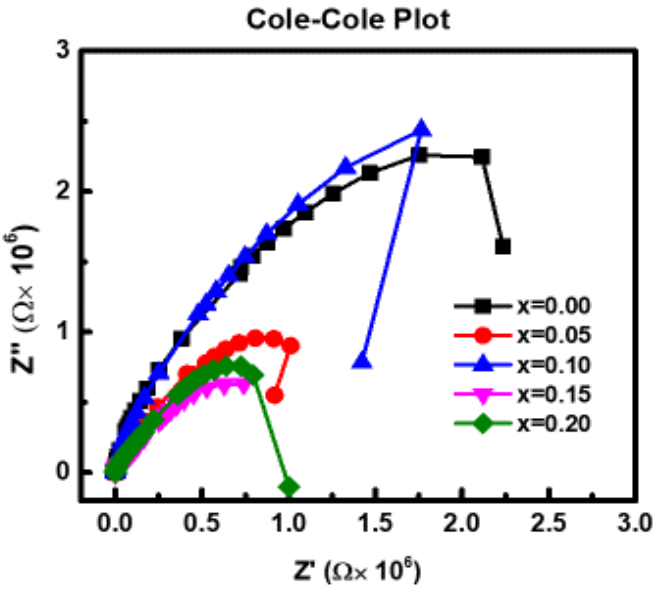

Fig. 4.8: Cole-Cole plot $Ni_{0.6}Mn_{0.2}Zn_{0.2}Cr_xFe_{2-x}O_4$ ferrites.

4.4 Magnetic Properties of $Ni_{0.6}Mn_{0.2}Zn_{0.2}Cr_xFe_{2-x}O_4$ (x=0.00, 0.05, 0.10, 0.15, 0.20) ferrites

4.4.1 Magnetization

Figure 4.9 (a) displays the compositions' M-H loops. Table 4.2 provides the computed values for the for M_s, M_r, and H_c of the given samples. The magnetization value increases and achieves saturation when the applied magnetic field is raised to a particular field. The *M-H* loops for the examined samples up to 10 kOe are shown in the first quadrant in Fig. 4.9 (b).

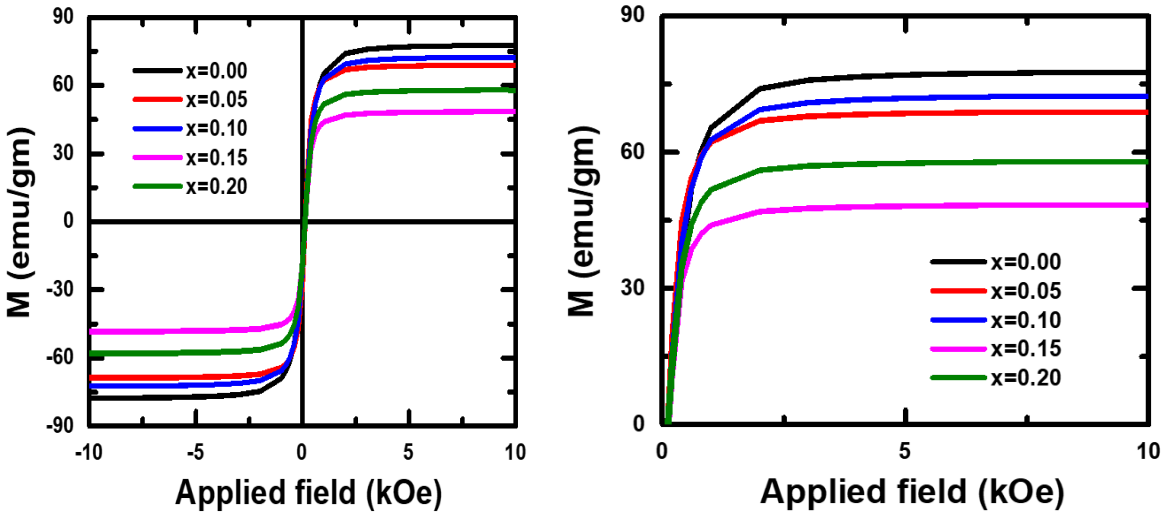

Fig. 4.9: (a) The M-H loops for $Ni_{0.6}Mn_{0.2}Zn_{0.2}Cr_xFe_{2-x}O_4$ (x=0.00 to x=0.20) compositions at (b) T_s=1000 °C; (b) 1st quadrant of M-H loop of NMZCFO compositions.

As the Cr^{3+} concentration rises, M_s value falls, falling between 77.55 and 48.42 emu/gm. The decrease of M_s can be explained based on the following equation: $M_s = |M_B - M_A|$; A and B sites' magnetic moments are shown by M_A and M_B, respectively. The Cr^{3+} ions are known to prefer B sites [32]. The magnetic moment of Cr^{3+} is less than that of Fe^{3+}. Therefore, the overall magnetic moment at the octahedral sites decreases when Fe^{3+} ions are replaced with Cr^{3+} ions. The total magnetic moment of the Cr-substituted ferrites

decreases as M_B decreases in the equation above. Accordingly, it is expected that the Cr replacement would cause the M_s to drop, as it did in this instance. The decrement of M_s due to Cr^{3+} substitution is consistent with the literature [33].

Table 4.2: The computed saturation magnetization (Ms), remanent magnetization (Mr), and coercive field (Hc) of $Ni_{0.6}Mn_{0.2}Zn_{0.2}Cr_xFe_{2-x}O_4$ (x=0.00 to 0.20) ferrites.

X content	M_s (emu/gm)	M_r (emu/gm)	H_c (O_e)
0.00	77.55	25.068	15.572
0.05	68.81	30.336	14.333
0.10	72.37	11.776	7.533
0.15	48.42	19.733	13.543
0.20	57.91	25.62	15.183

It is clear that adding Cr^{3+} ions during the magnetization and demagnetization operations, the M-H loop requires additional energy, yet the coercive field decreases as Cr^{3+} ions are added, from 15.572 Oe to 7.533 Oe, because the isotropic field becomes less intense [33,34]. As the $Ni_{0.6}Mn_{0.2}Zn_{0.2}Cr_xFe_{2-x}O_4$ ferrite composition with Cr^{3+} concentration rises, the value of H_c falls (Table 4.2).

Hysteresis curves are employed to discern the distinctions between delicate magnetic substances and rigid magnetic objects. For materials with strong magnetic properties, the location of the hysteresis loop is big because it indicates the quantity of magnetic energy that may be harnessed to accomplish work. However, while dealing with a delicate magnetic substance, the enclosed region within the hysteresis loop is sufficiently diminutive, resulting in a minimal dissipation of energy due to the repetitive reversal of magnetization. Lower coercivity soft magnetic materials were created, as confirmed by the hysteresis loops in this work [35].

4.4.2 Permeability

In Fig. 4.10, we can see the initial permeability of toroid-shaped samples at different frequencies. Up until approximately 30 MHz, a nearly constant μ' is noted before abruptly decreasing to a low level. This consistent value is essential for several applications, including transformers used for broadband pulses and read-write heads in wideband video recording systems [36].

In the produced samples, the permeability similarly falls gradually with Cr substitution. The decline in the initial permeability of the Ni-Mn-Zn ferrites can be elucidated by the equation $\mu' = \frac{M_S^2 D}{\sqrt{K_1}}$, where μ', Ms, D, and K denote the initial permeability, saturation magnetization, average grain size, and anisotropy constant, respectively. The saturation magnetization exhibited a drop as the Cr^{3+} substitution increased, which is usually ascribed to the diminished strength of the A-O-B super-exchange connections. Consequently, this led to a decrease in the value of μ' [37].

Variations in grain size affect the rotation of the domain and the displacement of the domain barrier, both of which modify the initial permeability of the samples. Because the initial permeability drops for x= 0.05 and x = 0.10 prohibit the domain barrier displacement, the Cr^{3+} ions are initially stuck in the grain borders. The permeability in the $Ni_{0.6}Mn_{0.2}Zn_{0.2}Cr_xFe_{2-x}O_4$ ferrites increases at x > 0.10 [but still lower than the parent composition] with increasing ions of Cr^{3+} because larger grains allow for easier movement of the domain barrier than before.

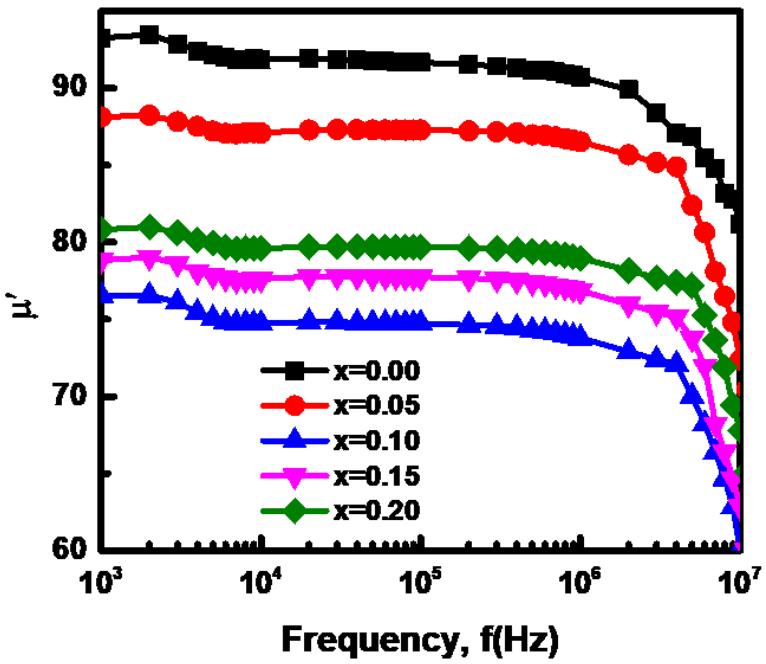

Fig. 4.10: Permeability $Ni_{0.6}Mn_{0.2}Zn_{0.2}Cr_xFe_{2-x}O_4$ ferrites for various compositions is frequency dependent.

4.4.3 Quality Factor

When assessing a sample's performance in real-world applications, the quality component is an important metric. The diagram demonstrates the correlation between frequency and relative quality parameters.

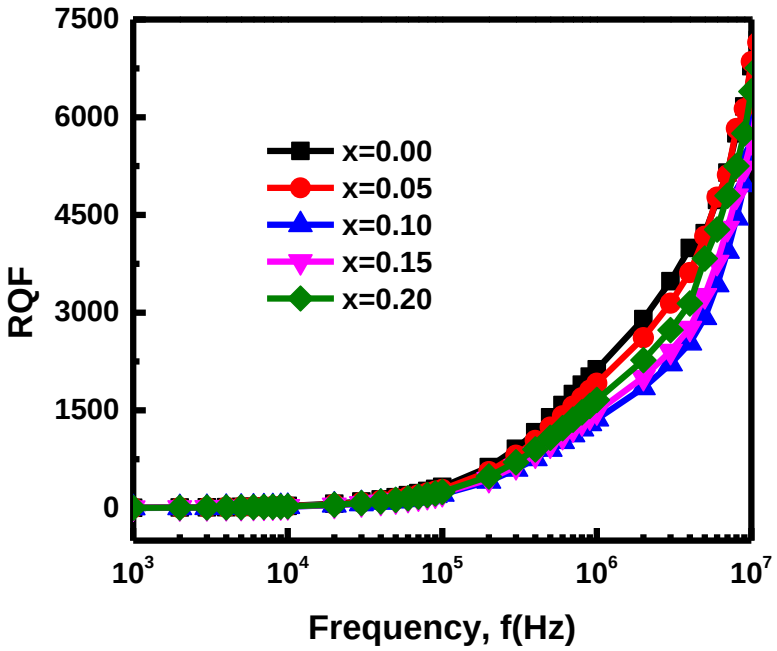

Fig.4.11: Frequency versus RQF plot for $Ni_{0.6}Mn_{0.2}Zn_{0.2}Cr_xFe_{2-x}O_4$ ferrites.

According to Fig. 4.11, it can be shown that the quality factor of $Ni_{0.6}Mn_{0.2}Zn_{0.2}Cr_xFe_{2-x}O_4$ ferrites exhibits an upward trend as the frequency increases. Moreover, at higher frequencies, ferrites with chromium substitution demonstrate superior quality compared to lower frequency sides.

References

[1] O.M. Hemeda, M.M. Barakat. Journal of magnetism and magnetic materials. 223(2001), 2, 127-132.

[2] F. Alam, B. C. Das, A. K. M. Akther Hossain, Proceedings of 14th Global Engineering and Technology Conference ,29-30 December 3017, BIAM Foundation,63 Eskaton, Dhaka, Bangladesh.

[3] B.D. Cullity, "Elements of X-ray diffraction", (Addison-Wesley Publishing Company. Inc. Reading, Massachusetts, U.S.A.), 1956. 99.

[4] J B Nelson and D P Riley. Proceedings of the Physical Society, London, 57 (1945), 3, 160.

[5] O.M. Hemeda, M.M. Barakat. Journal of Magnetism and Magnetic Materials. 223(2001), 127-132.

[6] Bade Venkata Suresh, G.V.R. Seshagiri Rao, E. Nirmala Devi, Govind Nandipati, Inorganic Chemistry Communications,165 (2024) 112534,

[7] M. Chebbi , S. Mansouri · S. Hcini, C. Bouzidi , N. Hamdaoui , L. El Mir, Journal of Electronic Materials 54 (2025), 1475–1488.

[8] M.M. Rahman, M.S. Sheak, S. Pervin, N. Uddin, F. Ahmed, M.A. Hossain, M. Rahaman, M.S. Bashar, T. Hossain, S. Akhter. Journal of Bangladesh Academy of Sciences. 36 (2012), 199–212.

[9] [S. Ramesh, L.N. Patro, B. Dhanalakshmi, B. Chandrasekhar, T. Anil Babu, K. Chandra Babu Naidu, B. Parvatheeswara Rao, Materials Chemistry and Physics, 306 (2023), 128055.

[10] A.K. Subramanim, K. Kondo, M. Tada, M. Abe, M. Yoshimura, and N. Matsushita. Journal of Magnetism and Magnetic Materials. 321 (2009), 3979-3983.

[11] M.A. Gabal, Y.M.A. Angar. Journal of Magnetism and Magnetic Materials. 322 (2006), 3159-3165.

[12] ImageJ software link: https://imagej.en.softonic.com.

[13] K. Katsmi, S. Mamoru , I. Tatrsuo, I. Katsuya. Bulletin of the Chemical Society. 48 (1975), 1764.

[14] D.C. Sinclair, A.R. West. Journal of Applied Physics. 66 (1989), 3850.

[15] M.A. El-Hiti. Journal of Magnetism and Magnetic Materials. 192 (1999), 305.

[16] E. Melagiriyappa, H.S. Jayanna, B.K. Chougule**.** Materials Chemistry and Physics**.**

112 (2008), 68.

[17] S.F. Mansour, M.A. Abdo, S.I. El-Dek. Journal of Magnetism and Magnetic Materials. 422 (2017), 105.

[18] M. Hashim, S.S. Meena, R.K. Kotnala, S.E. Shirsath, P. Bhatt, S. Kumar, E. Sentürk, R. Kumar, A. Alimuddin, N. Gupta. Journal of Magnetism and Magnetic Materials. 360 (2014), 21.

[19] M.A. Ali, M.M. Uddin, M.N.I. Khan, F.U.Z. Chowdhury, S.M. Hoque, Journal of Magnetism and Magnetic Materials. 424 (2017), 148.

[20] M.A. Ali, M.N.I. Khan, F.U.Z. Chowdhury, S. Akhter, and M.M. Uddin. Journal of Scientific Research. .7 (2015), 65.

[21] C.G. Koops. Physical Review. 83 (1951), 121.

[22] J.C. Maxwell. Electricity and Magnetism. Oxford University Press, New York. 1973.

[23] M. Hijchstiidter. Current Applied Physics. 14 (2014), 12, 1727–1733.

[24] C. G.Koops, Physical review .83 (1951), 121–124.

[25] G.S. Luo, W.P. Zhou, J.D. Li, G.W. Jiang, S.L. Tang, Y.W. Du. Journal of Materials Science: Materials in Electronics. 29 (2018), 12489−12495.

[26] K. Verma, A. Kumar, D. Varshney. Current Applied Physics. 13 (2013), 467.

[27] V.R.K. Murthy, J. Sobhanadri. Physical Status Solidi A. 36 (1976) K133.

[28] J.R. Macdonald. Impedance Spectroscopy: Emphasizing Solid State Material and Systems, (Wiley, NewYork), 1987.

[29] K.P. Padmasree, D.D. Kanchan, A.R. Kulkami. Solid State Ionics. 177 (2006), 475.

[30] E. Pervaiz and I H Gul. Journal of Physics: Conference Series 439 (2013), 012015.

[31] M.V. Chaudhari, S.E. Shirsath, A.B. Kadam, R.H. Kadam, S.B. Shelke, D. R . Mane. Journal of Alloys and Compounds. 552 (2013), 443–450.

[32] I.H. Gul, A.Z. Abbasi, F. Amin, M. Anis-ur-Rehman, A. Maqsood. Journal of Magnetism and Magnetic Materials. 311 (2007), 494-499.

[33] A.Y. Sleem, N.I. Abu-Elsaad, S.A. Mazen, Bulletin of Faculty of Science, Zagazig University (BFSZU),2023, 1, 24- 31.

[34] M. Raghasudha, D. Ravinder, and P. Veerasomaiah. Journal of Chemistry. 2013 (2013), 1, Article ID: 804042, 6.

[35] K. Sun, Journal of Magnetism and Magnetic Materials. 320 (2008), 1180.

[36] K. Ashok, B. Masin, Sreemoolanadhan, Hand Mathew, Transactions of the Indian Ceramic Society. 78 (2019) 1.

[37] X.F. Fan, H.P. Ren, Y.H. Zhang, S.H. Guo, X.L. Wang. Rare Metals. 27 (2008), 287-291.

Chapter 5: Conclusions

Efforts are being undertaken to address the issues posed by the developments in ferrite technology. The investigation and analysis of the potential fluctuations in the structural, electrical, and magnetic characteristics of cubic spinel $Ni_{0.6}Mn_{0.2}Zn_{0.2}Fe_{2-x}Cr_xO_4$ *ferrites resulting from the replacement of Fe ions by Cr ions have been conducted. The results acquired in this study are succinctly described in the subsequent summary observes:*

5.1 Conclusions

The mixed spinel ferrite $Ni_{0.6}Mn_{0.2}Zn_{0.2}Cr_xFe_{2-x}O_4$, x=0.00 to 0.20 in steps of 0.05, was synthesized through the use of traditional solid-state reaction strategies.

- The cubic spinel structure is confirmed by the XRD pattern, and the replacement of Cr results in a reduction in the lattice parameter. The density has also been changed significantly due to Cr substitution.
- The SEM measurements validate a uniform appearance of the grain dimensions. The grains are found to be decreased due to Cr substitution, except for x = 0.10.
- The frequency-dependent dielectric constant exhibits the usual ferrite nature. An increment in the dielectric constant is found due to Cr substitution.
- Study of electric modulus confirms the charge carriers' shift from long-range to short-range arrangement.
- Impedance spectroscopy analysis shows the dominant role of the grain boundary within the studied samples.

- The significance of coercive field, remanent magnetism, and saturation magnetization decreases after chromium substitution in Ni-Mn-Zn ferrites.
- Permeability decreases with increasing Cr substitution.

5.2 Suggestions for Further Research

In order to effectively apply practical implementations, thorough research is essential. The distribution of cations on tetrahedral and octahedral sites determines the electrical and magnetic characteristics of spinel ferrites. Neutron diffraction analysis serves as a valuable method for accurately identifying cation distribution. Additionally, exploring the dielectric properties across varying temperatures could provide insightful information. This approach would enhance the understanding of the samples' electrical behaviors.